Submitted to International Journal of Coal Geology

Optimum and robust 3D facies interpolation strategies in a heterogeneous coal zone

(Tertiary As Pontes basin, NW Spain)

Oriol Falivene*, Lluis Cabrera, Alberto Sáez

Geomodels Institute. Group of Geodynamics and Basin Analysis. Dept. of Stratigraphy, Paleontology and Marine Geosciences. Universitat de Barcelona, c/ Martí i Franques s/n, Facultat de Geologia, 08028 Barcelona, Spain.

Abstract:

Coal exploration and mining in extensively drilled and sampled coal seams can benefit from 3D statistical facies interpolation. Starting from closely spaced core descriptions, and using interpolation methods, a 3D optimum and robust facies distribution model was obtained for a thick, heterogeneous coal seam zone deposited in the non-marine As Pontes basin (Oligocene-Early Miocene, NW Spain). Several grid layering styles, interpolation methods (truncated inverse squared distance weighting, truncated kriging, truncated kriging with an areal trend, indicator inverse squared distance weighting, indicator kriging, and indicator kriging with an areal trend) and searching conditions were experimented and the results compared. Facies interpolation strategies were evaluated using visual comparison and cross validation. Moreover, robustness of the resultant facies distribution with respect to variations in interpolation method input parameters was verified by taking into account several scenarios of uncertainty. The resultant 3D facies reconstruction improves the understanding of areal distribution and geometry of the coal facies. Furthermore, since some coal quality properties (e.g. calorific value or sulphur percentage) display a good statistical correspondence with facies, predicting the distribution of these properties using the

* *Corresponding author: Tel: +34 934034028; Fax: +34 934021340; Mail address: oriolfalivene@ub.edu*

Submitted to International Journal of Coal Geology

3D facies distribution in a heterogeneous coal seam zone (As Pontes basin, NW Spain). Optimum and robust facies interpolation strategies

Oriol Falivene*, Lluis Cabrera, Alberto Sáez

Geomodels Institute. Group of Geodynamics and Basin Analysis. Dept. of Stratigraphy, Paleontology and Marine Geosciences. Universitat de Barcelona, c/ Martí i Franques s/n, Facultat de Geologia, 08028 Barcelona, Spain.

Abstract:

Coal exploration and mining in extensively drilled and sampled coal seams can benefit from 3D statistical facies interpolation. Starting from closely spaced core descriptions, and using interpolation methods, a 3D optimum and robust facies distribution model was obtained for a thick, heterogeneous coal seam zone deposited in the non-marine As Pontes basin (Oligocene-Early Miocene, NW Spain). Several grid layering styles, interpolation methods (truncated inverse squared distance weighting, truncated kriging, truncated kriging with an areal trend, indicator inverse squared distance weighting, indicator kriging, and indicator kriging with an areal trend) and searching conditions were experimented and the results compared. Facies interpolation strategies were evaluated using visual comparison and cross validation. Moreover, robustness of the resultant facies distribution with respect to variations in interpolation method input parameters was verified by taking into account several scenarios of uncertainty. The resultant 3D facies reconstruction improves the understanding of areal distribution and geometry of the coal facies. Furthermore, since some coal quality properties (e.g. calorific value or sulphur percentage) display a good statistical

* *Corresponding author: Tel: +34 934034028; Fax: +34 934021340; Mail address: oriolfalivene@ub.edu*

correspondence with facies, predicting the distribution of these properties using the reconstructed facies distribution as a template proved to be a powerful approach, yielding more accurate and realistic reconstructions of these properties in the coal seam zone.

Keywords: *3D facies interpolation, indicator kriging, areal trend, coal seam, cross validation*

1. Introduction

1.1. Problem statement

Many efforts have been devoted to the assessment of coal resources through 2D interpolations, either by using thickness maps (Starks et al., 1982; Journel and Rossi, 1989; Schuenemeyer and Power, 2000; Hohn and McDowell 2001; Tercan and Karyigit, 2001) or percentage maps showing distribution of coal quality properties (Davis and Greenes, 1983; Bancroft and Hobbs, 1986; Watson et al., 2001; Turner and Richardson, 2004). Such approaches provide useful predictions when dealing with homogeneous coal seams, as well as for the general assessment of reserves.

In the case of heterogeneous coal seam zones, closely and regularly spaced 2D cross sections or depth slices are also useful to manage coal exploration and mining. Nevertheless, 3D interpolation will deliver better results because it enables to integrate larger amounts of information in an efficient and optimum manner. Interpolation results include a 3D visualization capturing coal seam zone complexity, that can be further used for refining exploration and mining. Interpolation is applied in many earth sciences disciplines. Herein is used to obtain pixel-based property reconstructions by estimating the values of a given property at the cells of a grid (Jones et al., 1986). Several

interpolation strategies and methods exist; however, to the authors' knowledge these have not been widely applied to the analysis of facies distribution in coal seam deposits.

1.2. Aims

This study aimed at comparing and testing several strategies for the 3D interpolation of facies distribution. The case study chosen for this is the so-called coal seam zone 6AW, a thick, heterogeneous coal dominated interval that has been extensively drilled and mined in the As Pontes basin (Oligocene-Early Miocene, NW Spain).

Interpolation strategies were defined based on the variation of three crucial aspects: 1) the grid layering style, 2) the interpolation method, and 3) the number of data points averaged in order to obtain each estimated grid cell (searching conditions). Optimum and robust 3D interpolation strategies were derived using visual comparison and cross validation (CV). Optimality herein refers to reconstruction of facies distributions that show a realistic geological appearance and minimal CV errors and smoothing. Robustness refers to a solution that is stable respect to variations in the interpolation method input parameters. Robustness was evaluated by considering different scenarios of input parameter uncertainty.

This paper proves that 3D facies reconstruction improves the comprehension of spatial facies distribution and mutual relationships. In addition, since some coal quality properties (e.g. calorific value or sulphur percentage) can be often correlated with facies, the 3D facies distributions obtained through interpolation were also tested as a template for obtaining more accurate and realistic distributions for these properties.

2. Setting

2.1. Geological setting

The small (12 km^2), non-marine As Pontes basin resulted from the activity of an Oligocene-Early Miocene strike-slip fault system (Santanach et al., 1988, 2005) Fig. 1A). During the early evolutionary stages of this system two subbasins developed (Eastern and Western), bounded by contractive and extensional structures (Ferrús, 1998; Santanach et al., 2005, Fig 1B to 1D). The basin infill in both subbasins resulted from the interaction of sedimentation in alluvial fans and lacustrine to marsh-swamp systems, and consists of brown coal seams together with siliciclastic facies assemblages (Bacelar et al., 1988; Cabrera et al., 1995, 1996; Ferrús, 1998, Fig. 1C).

The basin infill has been split into 5 major genetic stratigraphic units (Ferrús, 1998; Sáez and Cabrera, 2002, Fig. 1C). Unit 1 in the Western subbasin and Units 2 to 5 in both basins are made up by several coal bearing composite sequences. Each composite sequence includes a lower interval, which is made up of a widespread, nearly basin-wide coal seam that interfingers with siliciclastic alluvial and lacustrine successions along the basin margins. This coal-bearing interval is overlain by an upper coal barren interval, which is dominated by major sandy and mudstone deposits resulting from an extensive basinward alluvial fan spreading. These composite sequences are bounded by isochronous or near-isochronous surfaces related to the settling and quick spreading of the major coal seams (Fig. 1C).

The coal seam zone 6AW is located in the upper part of Unit 1 and makes up the lower interval of the sixth composite sequence in the Western subbasin (Fig. 1C). Deposition of 6AW took place in well-developed marshes and swamps related to areally

very restricted marginal alluvial and lacustrine zones, where close interfingering between mudstone and coal deposits occur. Simultaneously, sedimentation in the Eastern subbasin resulted from the interplay between alluvial fan and shallow to deeper lacustrine zones where no coal accumulated (Fig. 1C and 1D; Cabrera et al., 1995; Sáez and Cabrera, 2002). The 6AW coal zone is about 30 m thick in average and reaches its maximum thickness (~50m) towards the northern basin margin. These coal deposits are thickest in the northern and central zones of the Western subbasin, but also onlap the basement toward the southern Western subbasin margin, and reached a maximum areal extent of 2.5 km^2 during the late depositional stages of 6AW (Fig 1D).

2.2. The coal seam zone facies

The As Pontes basin coal deposits can be classified as low mature lignite B (ASTM) or class 11/12 (UN-ECE), with huminite reflectance (ranging from 0.31% to 0.39%), and relatively high to very high ash contents and low to moderate calorific values (Cabrera et al., 1995). Coal deposition took place in diverse marsh-swamp environments where a diversity of tropical vegetal communities developed (Cavagnetto, 2002). Ash and total sulphur percentages in the As Pontes basin coal deposits, and particularly in the 6AW zone, are high if compared to other commercial coals. These characteristics resulted from both the alluvial fan influence and the probably closed-restricted basin drainage conditions, which led to the significant sulphate inputs into the basin to be captured in the anoxic peat forming environments (Huerta et al., 1997; Huerta, 1998, 2001).

Three major coal facies makes up most of the 6AW deposits: a) dark brown coal (DBC), b) pale yellow brown coal (PBC), and c) xiloid brown coal (XBC). These facies have been described elsewhere (Cabrera et al., 1992, 1995; Hagemann et al., 1997;

Huerta et al., 1997; Huerta, 1998, 2001). The DBC is a huminite dominated, often very biodegraded brown coal generated in subaerial to shallow subaqueous marshes and arbored swamps. The PBC is a liptinite-rich brown coal resulting from the accumulation of highly degraded aquatic and marsh plant remains. These accumulations would be deposited either under perennial or ephemeral shallow subaqueous water conditions (open aquatic marshes; Huerta, 1998). The XBC records the accumulation of middle to large sized wood remnants, either in place on forested swamps or slightly transported to neighbouring areas by low-energy currents and then randomly deposited (Huerta, 1998).

Two minor mudstone facies occur interbedded and interfingered with the coal facies: a) light coloured, grey to brown alluvial massive mudstones (AM) and b) green massive to dark thinly bedded lacustrine mudstones and shales (LM). AM record sedimentation in the distal and marginal zones of the alluvial fans that impigned from the basin margins and surrounded the peat-forming environments (Fig. 1D). LM record deposition in relatively stable shallow to deeper lacustrine zones, which were subject to intense detritic input from the marginal alluvial fans and changing organic matter contribution. The relatively deeper water conditions compared to mire zones and the detritic input would have inhibited peat accumulation.

Coal facies (DBC, PBC and XBC) show frequent vertical contacts and transitions as well as lateral interfingering among them and with the siliclastic facies (AM and LM). This fact is due to the complex and varied paleonvironmental evolution, and resulted in a complex spatial facies distribution that is difficult to capture through 2D analysis. As a consequence, the 3D interpolation was considered a powerful approach to improve the visualization and the comprehension of the facies distribution of the coal seam zone.

2.3. The data set

Owing to its economic interest as a coal basin, the As Pontes basin infill has been extensively drilled. Core descriptions of the wells drilled through the 6AW coal seam zone were used as the input data for this study (Fig. 2). These were complemented with surface observations and further study and sampling of the coal seam outcrops in the open pit mining trenches (Cabrera et al., 1992, 1995; Hagemann et al., 1997; Huerta et al., 1997; Huerta, 1998, 2001).

A total of 174 wells, amounting approximately 4000 meters of core description, were available for 6AW. Wells were drilled along a nearly regular square grid with a spacing of approximately 105 m (Fig. 2). Core descriptions, recorded by ENDESA MINA PUENTES, resolved beds over 0.15 m thick. For this study original descriptions were simplified to 5 representative facies taking into account the results of the lithological-textural and petrological analyses; these facies display diverse development in terms of percentage in the 6AW cores: LM (3%), PBC (12%), DBC (53%), XBC (7%) and AM (25%).

Besides facies records, the dataset also includes coal quality properties (moisture, ash content, volatile matter, calorific value and sulphur percentage). These data have been used to test the correlation of the three major coal facies with some of their characteristics. The results show that in some cases a good statistical correspondence exists, for example XBC is characterized by higher calorific values than PBC and DBC (Fig. 3A), whereas DBC is characterized by higher sulphur percentages than XBC and PBC (Fig. 3B), both on a dry base.

3. Methodology for interpolation strategies

Interpolation provides a unique and smooth property distribution honouring input data and aiming at local accuracy (Isaaks and Srivastava, 1989; Journel et al., 2000). The most common interpolation methods obtain the estimated values for a property at any given point by averaging nearby sampled property values. Weighting for each data point averaged may be assigned according to inverse of distance criteria or spatial covariance criteria (kriging-based methods; Journel, 1986).

3.1. Continuous property interpolation methods background

Continuous properties take real or integer values ordered continuously (e.g. thickness, sulphur percentage…). Interpolation methods have been widely used to map these properties. The search for optimum interpolation strategies has resulted in a large number of comparative studies based on visual appearance, CV results (i.e. a statistical test based on estimating the property value at locations where the true value is known, but has been temporally removed from the input data, and comparing the estimated values to the true data in order to judge the goodness of the estimation strategy, Isaaks and Srivastava, pp. 351-368, 1989), or measures of further responses (which are based on the interpolated property). Most of these studies have been applied to natural or synthetic properties defined in 2D, and have yielded diverse results. In some cases, geostatistical kriging-based methods have performed better (Rouhani, 1986; Brummert et al., 1991; Weber and Englund, 1994; Borga and Vizzaccaro, 1997; Zimmerman et al., 1999; Goovaerts, 2000; Teegavarapu and Chandramouli, 2005), but in others, inverse distance weighting or splines methods have produced similar or even better results (Brummert et al., 1991; Weber and Englund, 1992; Boman et al., 1995; Borga and Vizzaccaro, 1997; Dirks et al., 1998; Moyeed and Papritz, 2002).

3.2. 3D geological categorical properties and general set up

Interpolations for facies distribution were carried out using shifted vertical coordinates transforming the top of 6AW to a horizontal datum. This enabled restoration of most of the structural deformation along the northern basin margin (Santanach et al., 2005), and allowed an easier visualization of facies distribution. When dealing with a geological property like facies defined in 3D, an additional critical aspect related to the geometry of the interpolation grid exists. 3D interpolation grids were built bounded by base and top surfaces. Each grid consists of a number of adjacent cells of parallepiped geometry. Sides of the cells are vertical and define a rectangular mesh, whereas bases and tops (i.e. the grid layering) may deviate from horizontal. Grid layering should be designed to mimic those planes along which facies display more continuity (i.e. paleodepositional surfaces or bedding, Jones, 1988), and reproduce tectonic and sedimentary arrangements such as onlap, offlap, burial effects and erosion. To illustrate the importance of grid layering it was considered useful to compare four different styles.

Contrasting to continuous properties, facies distribution is a typical example for a categorical property (Deutsch, 2002). Categorical properties take discrete values, which do not need to follow any ordering (i.e. from category A to category C a transitional step with category B may not exist). Due to the variety of results related to optimum interpolation strategies for continuous properties and the paucity of studies comparing strategies for categorical properties (de Marsily et al., 2005), it was considered useful to compare six different average-based interpolation methods for reconstruction of facies distribution. To illustrate the effect of the number of neighbours averaged in order to obtain each estimate seven different scenarios were considered.

A common feature to average-based interpolation methods is that the property at each grid cell is obtained independently of the other estimated cells enabling a faster use of CV test. It should be also noted that the standard deviation of the reconstruction is smaller than the standard deviation of the original input data (i.e. smoothing effect; Isaaks and Srivastava, 1989; Journel et al., 2000), whereas the spatial continuity (variogram range) is increased. In terms of facies reconstructions the smoothing effect implies that resultant facies proportions differ from those in the original input data, with an increase in the relative proportions of the most extended categories.

In summary, interpolation strategies, which are detailed below, were defined based on the following crucial aspects: 1) the grid layering style, 2) the interpolation method and 3) the searching conditions.

3.3. Grid layering style and grid construction

The four different grid layering styles compared in the 6AW coal zone were: a) layering parallel to the top of the coal zone (top layering, Fig. 4A), b) layering parallel to the base of the coal zone (base layering, Fig. 4B), c) layering proportional between the top and the base of the coal zone (proportional layering, Fig. 4C) and d) a combined layering approach (geological layering, Fig. 4D). For geological layering, a proportional layering was used in the centre of the basin and its northern and eastern active basin margins, and parallel to top layering (i.e. horizontal) was used for the southern passive margin.

The vertical grid spacing was set to 0.15 m based on the resolution of core descriptions. In proportional and geological layering, cell thickness varied, but was equally set with a mean of nearly 0.15 m. Horizontally; the grid axes were aligned with

the positions of the wells (Fig. 2). The horizontal grid spacing was set to 20 m. Each grid cell can only have one facies assigned to it; therefore, facies described in the cores were upscaled to the size of grid cells. This was conducted for each layering style and by assigning the most abundant logged facies to each cell. Upscaled categories were the input data for all subsequent interpolations.

3.4. Interpolation methods

The interpolation methods compared were based on: a) resolving the categorical property distribution as multiple truncations of a continuous property (truncated approach methods: truncated inverse squared distance weighting (TISDW), truncated kriging (TK), and truncated kriging with an areal trend (TK-T)), or b) on the indicator approach for categorical properties (indicator approach methods: indicator inverse squared distance weighting (IISDW), indicator kriging (IK), and indicator kriging with an areal trend (IK-T)) (Table 1). GSLIB code (Deutsch and Journel, 1998) was used for kriging-based methods; GSTAT package (Pebesma and Wesseling, 1998) was used for inverse distance-based methods.

3.4.1. Truncated approach methods

Methods based on the truncated approach start by transforming facies categories to a single continuous property. This requires a previous ordering of facies. In our case this was done following energy-related paleonvironment criteria (LM, PBC, DBC, XBC and AM). These methods compute the thresholds between facies; assuming a Gaussian distribution, the areas between thresholds correspond to the proportions measured in the upscaled well data (de Marsily, 1998). The next step is to assign to each facies a value

between their thresholds; constant values located in the centre of each category were used.

The continuous values assigned to well data were used to derive experimental variograms with standardized sills. Theoretical variogram models were adjusted to the experimental ones (Fig. 5). Differences in horizontal variograms along different azimuths were not significant, and thus, horizontal isotropic ranges were used. The vertical variogram sills did not reach the standard deviation of the continuous property (Fig. 5). This fact is explained by the presence of an areal trend, as not all the vertical wells encounter the full variability of facies distribution (Kupfersberger and Deutsch, 1999; Gringarten and Deutsch, 2001).

Interpolation of the continuous property was conducted using three different algorithms (inverse distance weighting, kriging, and kriging with an areal trend; see below). In all cases, the final step of truncated approach methods was to truncate the continuous property interpolation with the thresholds between facies categories.

Truncated inverse squared distance weighting (TISDW)

Interpolation of the continuous property was carried out using inverse squared distance weighting (Kane et al., 1982; Pebesma and Wesseling, 1998) and conditioned by the well data. As indicated by the relationship between vertical and horizontal variogram ranges (Fig. 5) an important geometric anisotropy exists (Kupfersberger and Deutsch, 1999). This anisotropy is typical of sedimentary deposits, and in inverse squared distance weighting was considered by multiplying the vertical coordinates by an anisotropy factor prior to the interpolation (Jones et al, 1986; Zoraster, 1996). In order to get a reasonable value for the anisotropy factor, the ratio between horizontal and vertical variogram ranges was used.

Truncated kriging (TK)

Interpolation of the continuous property was also carried out using ordinary kriging (Matheron, 1963; Journel and Huijberts, 1978; Cressie, 1990) and conditioned by the well data and the adjusted theoretical variograms (Fig. 5).

Truncated kriging with an areal trend (TK-T)

The presence of an areal trend (Gringarten and Deutsch, 2001), as demonstrated by vertical variograms not reaching the standard deviation of the continuous property (Fig. 5), motivated the use of an interpolation method considering this trend explicitly (TK-T). The areal trend was modelled following the decomposition into a mean and a residual, as suggested by Langlais et al (1993) and Deutsch (2002). The mean corresponds to a 2D map derived from the interpolation of averaged values of the continuous property along each well (Fig. 6). In the well data locations, the residual was obtained by subtracting the mean from the original transformed property.

Experimental variograms were derived from the residual property and standardized sills were used (Fig. 7). As expected, experimental vertical variograms of the residual property did not show strong indication of areal trends. Theoretical variogram models were adjusted to the experimental ones. Differences in horizontal variograms along different azimuths were not significant, and thus, horizontal isotropic ranges were used. Interpolation of the residual property was carried out using ordinary kriging (Matheron, 1963; Journel and Huijbregts, 1978; Cressie, 1990) and conditioned by the residual at well data locations and the adjusted theoretical variograms. The results of the residual property interpolations were added to the mean.

3.4.2. Indicator approach methods

When dealing with categorical properties like facies, the indicator approach (Journel, 1983; Gómez-Hernández and Srivastava, 1990) transforms each facies into a new property, and the value of each new property corresponds to the probability of finding the related facies at a given position. Where well data exist, the value of the property corresponding to the facies present was set to one, whereas the values of the other properties were set to zero.

The transformed well data were used to estimate indicator variograms for each facies. In the case of indicator variograms, non-standardized sills were used, as the sill of an indicator variogram is related to the percentage of each facies. The theoretical variogram models were adjusted to the experimental ones (Fig. 8). Depending upon the spatial continuity shown by each facies, the horizontal and vertical variogram ranges varied. For each facies, differences in horizontal variograms along different azimuths were not significant, and therefore, horizontal isotropic ranges were used. The vertical variograms sills did not reach the standard deviation of the indicator properties (Kupfersberger and Deutsch, 1999; Gringarten and Deutsch, 2001); this effect was larger for facies DBC and AM (Fig. 8C and 8E). As in the case of the continuous approach, vertical variograms not reaching the sill are related to the presence of an areal trend.

Again, interpolation of the indicator properties was conducted using three different algorithms (inverse distance weighting, kriging, and kriging with an areal trend; see below). Results from the interpolation of indicator properties corresponded to the probability of finding each facies at each grid cell, and the final step of indicator

approach methods was to select the facies with the highest probability of occurrence at each grid cell.

Indicator inverse squared distance weighting (IISDW)

Interpolation of each new indicator property was carried out using inverse squared distance weighting and conditioned by the transformed well data. As horizontal and vertical variogram ranges varied depending upon the facies (Fig. 8), geometric anisotropy and the ratio between horizontal and vertical range also varied. Therefore, different anisotropy ratios were used for each facies.

Indicator kriging (IK)

Interpolation of each new indicator property was also carried out using ordinary kriging (Matheron, 1963; Journel and Huijbregts, 1978; Cressie, 1990) and conditioned by the transformed well data and the theoretical indicator variograms (Fig. 8).

Indicator kriging with an areal trend (IK-T)

The presence of an areal trend (Gringarten and Deutsch, 2001), as demonstrated by vertical indicator variograms not reaching the sill value (Fig. 8), motivated the use of an interpolation method explicitly considering this trend (IK-T). Areal trends for each facies were modelled following the same approach as for the continuous approach.

For each new indicator property, 2D mean maps were derived from the interpolation of averaged values along each well (Fig. 9). These maps corresponded to the areal proportion of each facies, and showed a clear non-stationary distribution. In the well data locations, for each indicator property, residuals were obtained by subtracting the mean maps to the original indicator properties.

Experimental variograms were derived from the residual properties, each corresponding to a different facies, and standardized sills were used. As expected, experimental vertical variograms of the residual properties did not show strong indication of areal trends (Fig. 10). The theoretical variogram models were adjusted to the experimental ones (Fig. 10). Differences in horizontal variograms along different azimuths were not significant for each facies, and thus, horizontal isotropic ranges were used. Interpolation of the residual properties was carried out using ordinary kriging (Matheron, 1963; Journel and Huijberts, 1978; Cressie, 1990) and conditioned by the residual properties at well data locations and the adjusted theoretical variograms (Fig. 10). The results of the residual properties interpolations were added to the mean maps for each facies.

3.5. Searching conditions

Searching conditions refer to the number of neighbouring data points averaged to obtain each grid cell estimate (NN). In this study, octant restrictions were not used since the input well data was already distributed over a nearly regular grid. The seven different NN scenarios used were: 4, 12, 24, 48, 96, 192 and 288.

4. Methodology for comparison criteria

Interpolation strategies were compared based on the geological realism of facies reconstructions and CV results (i.e. looking for minimum CV error and minimum CV smoothing).

4.1. Definition of the cross validation error

Several variations in the CV procedure and the error definition exist (Davis, 1987; Isaaks and Srivastava, 1989). In the case of categorical properties defined from well data, the following procedure was used to cross validate the results. First, an entire upscaled well was temporally extracted from input data. Second, facies interpolations were carried out on the grid cells intersected by the extracted well using the remnant data. Third, the predicted facies distribution in the extracted well was compared to the true distribution. This procedure was repeated for all the wells. The probability of obtaining an erroneous facies prediction was obtained by averaging results for all the grid cells intersected by the wells. Each grid cell was assigned the same weight, independently of its thickness. This CV error definition is a variant of the commonly used mean absolute error (Zimmermann et al., 1999; Teegavarapu and Chandramouli, 2005) adapted to categorical variables defined in 3D by well data. In all cases, the theoretical variogram models fitted with the complete data set were used (Figs. 5, 7, 8 and 10). For interpolation methods using areal trends (TK-T and IK-T), the areal trends were derived from the remnant wells when computing CV results.

4.2. Cross validation error and smoothing effect

Smoothing effect related to each interpolation strategy (defined by grid layering style, interpolation method and searching conditions) influences the probability of an erroneous facies prediction. Smoothing was measured herein by measuring the proportion of the most extended category (DBC) predicted by CV. Proportion of DBC as estimated from CV was larger and directly related to the proportion of DBC as estimated from a complete 3D facies interpolation (Fig. 11A). This is because mean distances between cross-validated locations and averaged data points are always larger

in CV than mean distances between estimated grid cells and averaged data points for a facies interpolation along the entire grid. This increase in average distance limits the use of CV error as an exact measure for interpolation accuracy, even though it can be used as an approximation or as a relative measure for ranking interpolation strategies.

Considering randomly generated facies estimates, it can be observed that the probability of obtaining erroneous predictions decreases as the smoothing effect increases (Fig. 11B). However, excessive smoothing should be avoided, since it would imply an artificial increase in spatial continuity of the facies distributions and an additional decrease of global accuracy (Goovaerts, 1997; Journel et al., 2000; Yamamoto, 2005). For any given degree of smoothing, CV interpolation errors were in all cases lower than the errors obtained using randomly generated unconditioned facies estimates (Fig. 11B).

5. Results

Visual analysis and CV test was conducted for 168 different interpolation strategies (4 grid layering styles, 6 interpolation methods and 7 NN scenarios).

5.1. Grid layering style

Visual appearance of facies reconstructions considering different grid layering styles is markedly different (Fig. 12). Fig. 13A shows CV results for indicator approach methods considering different grid layering styles and intermediate NN (48).

At the same smoothing degree, each grid layering style yield different randomly estimated CV errors (Fig. 11B). This effect is due to the use of CV results not corrected for cell thickness. Actually, layering styles show small differences in the upscaled facies

proportions not corrected by cell thickness, these differences are perfectly correlated to CV error (Fig. 14). In order to compare CV errors from different grid layering styles, the bias introduced by computing CV results without weighting for true thickness was removed. This was achieved by dividing CV errors by the CV error obtained using estimates with total smoothing (DBC facies proportion at 100%, i.e. mean mapping) (Fig. 13B).

In terms of CV errors corrected for cell-thickness, the worst layering style is that parallel to the base, independently of the interpolation method and searching conditions (Fig. 13B). This fact quantitatively reflects the importance of considering a nearly horizontal layering style for interpolation; recall that interpolation is carried out considering the top of the interval as a horizontal datum.

Parallel to the top, proportional and geological grid layering styles yield similar errors, with rankings differing depending on the interpolation method considered. For IK and IIDW the smallest errors are obtained by the proportional layering (Fig. 13B), whereas for IK-T the smallest error is obtained for the layering parallel to the top (Fig. 13B).

Based upon geological knowledge of the coal zone deposition and post-depositional evolution of the basin (Cabrera et al., 1995; Ferrús, 1998; Santanach et al., 2005) it is reasonable to consider the presence of post-depositional folded stratification in the central parts and in the northern active basin margins (Fig. 1 and 2); that makes the proportional and geological grid layering styles more appropriate (Fig. 12C and D). Differences in the geological and proportional layering are mostly limited to the southern passive basin margin, being geological layering the most realistic, because it reproduces the onlap typical of expansive zones like 6AW (Fig. 12D).

5.2. Interpolation method and searching conditions

Fig. 15 shows facies reconstructions for the different interpolation methods. Fig. 16 and 17 show CV results for the different interpolation methods and using different NN. Interpolation methods can be ranked based on the results for the more realistic geological and proportional grid layering styles (section 5.1). In nearly all cases, rankings are also valid for the other two grid layering styles (parallel to the base and parallel to top). Results can be summarized as:

1) As expected (Herzfeld et al., 1993), CV smoothing increases as NN increases (Fig. 16).

2) Truncated approach methods yield CV estimates with higher smoothing (71-95%) than indicator approach methods (57-82%) (Fig. 16).

3) CV errors show different patterns depending upon the interpolation method approach (Fig 16). Truncated approach methods yield more restricted errors (from 43% to 49%), than indicator approach methods (from 39 to 52%).

4) Considering only truncated approach methods: a) for small NN (4-12), TISDW performs better than kriging-based methods (Fig. 17A); b) for intermediate NN (48), CV error for TISDW remains slightly smaller than kriging-based methods error, but the smoothing is greater (Fig. 17B); c) for large NN (192-288), kriging-based methods perform better than TISDW (Fig. 17C); and d) except for small NN, TK-T yield better results than TK (Fig 17).

5) Considering only indicator approach methods: a) for small NN (4-12), kriging-based methods yield the smallest CV error, whereas the lowest smoothing correspond to IISDW (Fig. 17A); b) for intermediate to large NN (48-288), kriging-

based methods have the lowest smoothing, whereas IISDW have the lowest CV error (Fig. 17B and 17C); and c) in all cases IK-T yields lower smoothing than IK, whereas CV error depend on the NN (Fig. 17), for low NN (4-12), CV error is smallest for IK-T; and for intermediate to high NN (48-288), CV error is smallest for IK.

6) Indicator approach methods perform better than truncated approach methods (Fig. 16). Visual comparison also supports this result (Fig. 15); the facies distributions obtained with indicator methods appear more heterogeneous and realistic.

5.3. Method robustness

To study the sensitivity of the resultant facies reconstructions to variations in the method input parameters, four different anisotropy scenarios were compared: 1) the first scenario corresponded to an overestimation of horizontal variogram ranges by a factor of two, 2) the second scenario to the actual values measured from input data, 3) the third scenario to an underestimation by a factor of two, and 4) the fourth scenario to an underestimation by a factor of ten. No uncertainty in vertical variogram ranges was considered since it is usually well constrained by vertical wells.

Fig. 18 and 19 show respectively facies reconstructions and CV results considering the different uncertainty scenarios. Only the results for indicator approach, kriging-based methods, assuming a geological and proportional layering, and using NN set to 48 are shown. Results for truncated approach methods and inverse distance-based methods are not presented due to their limited optimality (section 5.2). Intermediate NN (48) provides an optimum balance between visual results, CV error and smoothing effect (section 5.2 and 6.2).

Relatively small changes (scenario 1 and 3) to the anisotropy measured from well data (scenario 2) do not significantly alter the appearance of resultant facies distributions (Fig. 18A, B and C). The only differences correspond to restricted variations in the facies continuity, with the first scenario yielding the most continuous results. Variations in facies continuity have a moderate impact on CV smoothing and CV error (Fig. 19); changes in the anisotropy are inversely proportional to smoothing and directly proportional to CV error. The fourth scenario provides visually different results (Fig. 18D). This scenario yields the lowest CV error, but at expenses of a higher smoothing and a non-realistic appearance. In all the uncertainty scenarios, IK-T yields lower CV smoothing than IK, but at expenses of a slight increase in CV error (Fig. 19).

6. Discussion

6.1. Grid layering style

Layering was used to preset the surfaces along which facies should display larger continuity, and in this study demonstrated a critical influence on the resultant facies distributions appearance and realism (Fig. 12). Grid layering must be assumed and is only necessary when dealing with 3D geological properties. This assumption should be strongly supported by a previous geological knowledge of the bedding attitude. As has been shown, CV can be used to verify the idoneity of the definition of grid layering.

6.2 Interpolation method and searching conditions

Indicator approach methods rank as the optimum for facies interpolation of the 6AW coal zone. Truncated approach methods produce the worst results; these methods

are based on simplifying facies distribution to a single variable. This simplification imposes: 1) continuous facies ordering, and 2) use of only one variogram or anisotropy factor to characterize spatial variability, with all facies sharing the same anisotropy (de Marsily et al., 1998). Truncated approach methods are useful mainly in depositional settings with a highly ordered facies distribution. On the other hand, indicator approach methods allow more flexibility in defining the spatial variability of each facies separately, but at the cost of an increase in the number of input parameters and the computing time roughly proportional to the number of facies considered.

Results for different indicator approach methods are very similar. From the visual comparison (Fig. 15) it was difficult to choose an optimal method. Method ranking using CV results is very sensitive to changes in NN. IIDW is the most sensitive method to variations in NN (Fig. 16). Similar results have been reported for interpolation dealing with continuous variables (Weber and Englund, 1992 and 1994). IK and IK-T are also sensitive to NN, but their CV error and CV smoothing stabilise beyond and intermediate NN (NN = 48, Fig. 16). Therefore indicator approach kriging-based methods were the preferred for facies interpolation (Fig. 17).

One of the most important advantages of kriging-based methods with respect to simpler inverse distance-based methods is the ability to take into account the relative positions of sampling data in order to select an optimal weighting scheme. This advantage is more significant when intermediate to high NN are considered. In addition, if input data were more irregularly distributed, differences in performance between kriging-based methods and inverse distance-based methods would increase.

An intermediate number of nodes (48) was chosen as an optimum compromise to minimize both CV error and smoothing effect (Fig. 16), and at the same time

obtaining a realistic facies distribution (Fig. 15). Using larger NN also implies a dramatically increase in computing time.

IK-T does not yield significantly better CV results than IK despite the presence of marked non-stationary facies distributions (i.e. areal trends). This agrees with results by Journel and Rossi (1989) dealing with a continuous variable. These authors stated that when interpolating using a limited NN, explicitly considering a trend does not significantly improve results obtained without explicitly considering the trend. This happens because in the latter case the trend is implicit when using a limited NN. Explicitly considering a trend proves more useful for extrapolation. In our study, the use of a trend with intermediate to large NN values (NN over 48) results in a diminution of CV smoothing, but at the expenses of a slight increase in CV error. The diminution of smoothing effect produced by the IK-T makes us consider it the optimum method for facies interpolation. The slight increase in CV error when explicitly using the trend agrees with the results by Zimmermann et al. (1999) dealing with a complex continuous variable.

6.3. Method robustness

Moderate errors in the determination of anisotropy (up to an overestimation or underestimation by a factor of two) do not significantly alter the results, confirming the robustness of the interpolation method. Large errors in the determination of anisotropy, particularly when corresponding to an underestimation, cause a large impact on the geological realism of the resultant facies distribution. However, such large errors are not likely to occur because interpolation is considered useful only when dense well data coverage is available, permitting a reasonable approximation to anisotropy. Hard data is the most important input for conditioning interpolation results.

6.4 The resulting 3D facies reconstruction

Once an optimum and robust 3D facies interpolation strategy was determined (IK-T using NN set to 48 and a geological grid layering style), the resultant 3D facies reconstruction was analysed. This reconstruction (Fig. 20A) allows a better understanding of spatial and geometrical relationships of facies (vertical and lateral changes, lateral continuity, coal seam splitting, etc).

The interaction between alluvial fans and the mire and lacustrine zones was the main factor controlling the areal development of the 6AW coal seam and the seam splitting by siliciclastic inputs. The areal distribution of the main environments in the coal zone (distal alluvial fan, marsh, swamp and lacustrine) varied during its deposition. These variations depended on the balance between allogenic factors (climate, tectonics and the resulting water and detritic inputs), as well as on the autogenic alluvial fan and mire evolution (Cabrera et al., 1995; Ferrús, 1998).

AM facies deposited in the distal and marginal zones of the alluvial fans that spread into the basin from its margins. Consequently this facies fringes the seam boundaries, particularly in the northern and eastern active basin margins, where small, fine-grained dominated alluvial fans developed related to tectonic structures (Fig. 1D and Fig. 20A). AM facies interfinger and even spread into the inner coal seam zone, causing its splitting. The 3D facies reconstruction allows us to recognize and trace these splitting zones precisely. This analysis is a powerful previous step to the accurate prediction and evaluation of the coal/mudstone rate changes that often occur as mining advances (Fig. 20A).

LM facies occur as isolated pods scattered along some marginal basin zones (Fig. 20A). The development and persistence of the small lakes where LM facies

deposited was probably favoured by a larger subsidence/sedimentation rate produced along the northern and eastern tectonic basin margins. However, their occurrence along the non-tectonically active southern margin also suggests the influence of other factors not yet fully understood. The resulting 3D reconstruction shows the occurrence of these coal barren zones that must be preventively considered during mining operations.

DBC facies makes up most of the coal seam and constitutes the dominant background. DBC beds are thick and laterally extensive and may spread all over the extent of the seam zone (Fig. 20A). PBC facies are a less important component in the seam zone. This facies often makes up laterally extensive but lenticular bodies that are embedded in the DBC dominated sequences. Exceptionally thick and persistent, laterally more restricted PBC sequences appear in the northeastern basin margin (Fig. 9 and 20A), which corresponds to one of the most subsiding areas during deposition of 6AW. The shallow subaqueous conditions suitable for deposition of PBC facies would developed persistently in this notheastern margin (where PBC attains its maximum thickness), and in some of the inner parts of the seam, far away from the detritic inputs that filled up the aquatic zones and prevented aquatic peat accumulation. The limited horizontal continuity of PBC facies is revealed by the 3D reconstruction and agrees well with the relatively small horizontal indicator variogram range (Fig. 8B). The XBC facies appears even as more randomly distributed than DBC and PBC and make up laterally restricted and mostly thin bodies (Fig. 20A). This conspicuous random distribution pattern accords well with the environmental conditions and processes that resulted in its deposition.

It is not possible to establish an obvious basinwide sequence evolutionary trend considering the relative DBC, PBC and XBC facies succession and development. In fact the local sequence evolutionary patterns are quite diverse in the different basin zones.

From this point of view the obtained 3D reconstruction arises as a powerful tool to capture the diverse facies distribution and the local variations of the facies-related coal properties (see section 6.5).

6.5. Interpolation of coal quality properties based on the 3D facies reconstruction

The facies reconstruction was also applied as a template to improve the realism and accuracy of coal quality property interpolations; this makes sense only when these properties depend at some extent on the facies category. In the case of the 6AW coals, a relationship between facies and calorific value (on a dry base) (Fig. 3A), and facies and total sulphur percentage (on a dry base) was observed (Fig. 3B).

Calorific value and total sulphur percentage interpolations were carried out using kriging with NN set to 48 and assuming a geological grid layering style. Two different interpolation strategies were compared: 1) interpolating the measured values of coal properties directly, without using facies as a template; and 2) interpolating facies and using the interpolated facies as a template to interpolate the values of the coal properties (i.e. taking into account the interpolated facies distribution in order to restrict averaged data points to those neighbours belonging to the same facies, Fig. 20B and C). Cross sections of the 3D interpolations are presented in Fig. 21 and 22. CV was used to quantitatively discriminate which strategy provides the most accurate coal property interpolations. When considering facies as a template two options were compared: a) using also cross-validated facies, and b) considering facies in the cross-validated well as already known.

The interpolations using facies as a template provide better CV results than the interpolations obtain without using facies (Table 2). Results using facies as a template

yield the lowest differences between the true mean and the interpolated distribution mean (conditional bias) and the true standard deviation and interpolated standard deviation (smoothing). Results using facies as a template also yield the lowest mean absolute error and relative mean absolute error (accuracy). CV results considering already known facies in the cross-validated wells are even better than the CV results using also cross-validated facies. The lower relative mean absolute errors yielded by calorific value respect to sulphur percentage (Table 2) is related to the fact that calorific value is better correlated to facies than sulphur, which is highly influenced by other factors (i.e. amount of sulphate inputs and redox conditions in each subbasin zone).

7. Conclusions

1) 3D interpolation permits the correlation of facies in a large number of wells. This technique proves to be useful when facies distribution is reasonably well captured by dense well data coverage.

2) Visual appearance and cross validation (CV) results prove to be valid tools to compare and rank different categorical property interpolation strategies and input parameter uncertainty scenarios. CV error is affected by the interpolation smoothing and tends to decrease as the smoothing increases.

3) The optimal and most robust facies interpolation strategy for the chosen case study (6AW coal seam zone, As Pontes basin) is indicator kriging with an areal trend (IK-T), using a number of data points averaged to obtain each estimate (NN) set to 48, and using a geological grid layering style.

4) An accurate definition of the grid layering style, based on *a priori* geological knowledge, prove very important to generate realistic facies reconstructions.

5) The indicator approach methods provide visually similar facies distributions. Results of indicator kriging (IK) are slightly less robust to variations in the input method parameters than results of IK-T, and indicator inverse squared distance results are more sensitive to variations in searching conditions than IK and IK-T. Truncated approach methods yield the worst results.

5) Smoothing effect increases with NN; intermediate NN values provide an optimum compromise between CV error, CV smoothing and computing time.

7) 3D interpolations provide a useful representation of facies distribution, which enables a better understanding of spatial and geometrical aspects of facies distribution in the coal seam zone.

8) As sulphur percentage and calorific value depend at some extent on coal facies, 3D facies reconstructions enables a more accurate interpolation of these properties.

9) This work demonstrates how 3D facies reconstructions are suitable and advisable for optimising coal exploration and mining in extensively drilled and sampled, thick and heterogeneous coal seam zones. Such reconstructions would help in planning selective mining according to the facies distribution and their related properties.

8. Acknowledgements

This research was carried out in the Geomodels Institute. This institute is sponsored by Generalitat de Catalunya (DURSI) and Instituto Geologico y Minero de España (IGME) and includes the 3D Geological Modelling CER (University of Barcelona). The authors are indebted to ENDESA MINA PUENTES for providing the dataset; its department of geology is also acknowledged for friendly support and field guidance. Financial support from the MEyC (Proyectos CARES BTE 2001-3650 and MARES CGL 2004-05816-C02-02/BTE) and from the Generalitat de Catalunya (Grup de Recerca de Geodinàmica i Anàlisi de Conques, 2005SGR-000397) is acknowledged. O. Fernández and Y. Almar are acknowledged for the review of a preliminary manuscript. Research by O. Falivene is funded by a pre-doctoral grant from the Spanish Government (Ministerio de Educación y Ciencia). Roxar is thanked for providing the IRAP RMS reservoir modelling software.

9. References

Bacelar, J., Alonso, M., Kaiser, C., Sánchez, M., Cabrera, L., Sáez, A., Santanach, P., 1988. La Cuenca Terciaria de As Pontes (Galicia): su desarrollo asociado a inflexiones contractivas de una falla direccional, Simposio sobre Cuencas en régimen transcurrente. Sociedad Geologica de España, pp. 113-121.

Bancroft, B.A., Hobbs, G.R., 1986. Distribution of kriging error and stationarity of the variogram in a coal property. Mathematical Geology 18, 635-652.

Boman , G., Molz, F.J., Guven, O., 1995. An evaluation of interpolation methodologies for generating three-dimensional hydraulic property distributions from measured data. Ground Water 33, 247-258.

Borga, M., Vizzaccaro, A., 1997. On the interpolation of hydrologic variables: formal equivalence of multiquadratic surface fitting and kriging. Journal of Hydrology 195, 160-171.

Brummert, A.C., Pool, S.E., Portman, M.E., Hancock, J.S., Ammer, J.R., 1991. Determining optimum estimation methods for interpolation and extrapolation of reservoir properties: a case study, in: Lake, L.W., Carroll, H.B., Wesson (Eds.), Reservoir Characterization, pp. 445-485.

Cabrera, L., Ferrús, B., Sáez, A., Santanach, P., Bacelar., J., 1996. Onshore Cenozoic strike-slip basins in NW Spain, in: Friend, P.F., Dabrio, C.J. (Eds.), Tertiary Basins of Spain, the Stratigraphic Record of Crustal Kinematics, pp. 247-254.

Cabrera, L., Hagemann, H.W., Pickel, W., Sáez, A., 1992. Caracterización Petrológica y Geoquímica Orgánica de los lignitos de la cuenca de As Pontes (La Coruña), II Congreso Geológico de España - VIII Congrso Latinoamericano de Geología. Tomo 2. Simposio sobre Geología del carbón, pp. 239-246.

Cabrera, L., Hagemann, H.W., Pickel, W., Sáez, A., 1995. The coal-bearing, Cenozoic As Pontes Basin (northwestern Spain): geological influence on coal characteristics. International Journal of Coal Geology 27, 201-226.

Cavagnetto, C., 2002. La plynoflore du Bassin d'As Pontes en Galice dans le Nord Ouest de l'Espagne à la limite Rupélien-Chattien (Oligocène). Palaeontographica. Abteilung B: Paläophytologie 263, 161-204.

Cressie, N., 1990. The origins of kriging. Mathematical Geology 22, 239-252.

Davis, B.M., 1987. Uses and abuses of cross-validation in geostatistics. Mathematical Geology 19, 241-248.

Davis, B.M., Greenes, K.A., 1983. Estimation using spatially distributed multivariate data: An example with coal quality. Mathematical Geology 15, 287-300.

de Marsily, G., Delay, F., Gonçalves, J., Renard, P., Teles, V., Violette, S., 2005. Dealing with spatial heterogeneity. Hydrogeology Journal 13, 161-183, DOI 110.1007/s10040-10004-10432-10043.

de Marsily, G., Delay, F., Teles, V., Schafmeister, M.T., 1998. Some current methods to represent the heterogeneity of natural media in hydrogeology. Hydrogeology Journal 6, 115-130.

Deutsch, C.V., 2002. Geostatistical Reservoir Modeling. Oxford, 376 pp.

Deutsch, C.V., Journel, A.G., 1998. GSLIB: Geostatistical Software Linrary and User's Guide, 2nd edition. Oxford University Press, 350 pp.

Dirks, K.N., Hay, J.E., Stow, C.D., Harris, D., 1998. High-resolution studies of rainfall on Norfolk Island Part II: interpolation of rainfall data. Journal of Hydrology. 208, 187-193.

Ferrús, B., 1998. Análisis de cuenca y relaciones tectónica-sedimentación en la cuenca de As Pontes (Galícia). University of Barcelona (Spain).

Gómez-Hernández, J., Srivastava, R.M., 1990. ISIM 3D: an ANSI-C three-dimensional and multiple indicator conditional simulation program. Computers & Geosciences 16, 355-410.

Goovaerts, P., 1997. Geostatistics for natural resources evaluation, New York, 483 pp.

Goovaerts, P., 2000. Geostatistical approaches for incorporating elevation into the spatial interpolation of rainfall. Journal of Hydrology 228, 113-129.

Gringarten, E., Deutsch, C.V., 2001. Variogram interpretation and modeling. Mathematical Geology 33, 507-535.

Hagemann, H.W., Pickel, W., Cabrera, L., Sáez, A., 1997. Tertiary lignites of the As Pontes (NW Spain) - An example for composition of bright coal layers and its implications for formation, Proceedings of the 9th International Conference on Coal Science, 1: 31-34.

Herzfeld, U.C., Eriksson, M.G., Holmund, P., 1993. On the Influence of Kriging Parameters on the Cartographic Output - A Study in Mapping Subglacial Topography. Mathematical Geology 25, 881-900.

Hohn, M.E., McDowell, R.R., 2001. Uncertainty in Coal Property Valuation in West Virginia: a case study. Mathematical Geology 33, 191-217.

Huerta, A., 1998. PhD Tesis. Petrografía, Mineralogía y Geoquímica de los lignitos de la cuenca Oligo-Miocena de As Pontes (A Coruña): Control geológico sobre la calidad del carbon, Universitat de Barcelona, pp. 333.

Huerta, A., 2001. Resumen de tesis Doctoral: Caracterización mineralógica y geoquímica de los lignitos de la cuenca Terciaria de As Pontes (Provincia de La Coruña). Acta Geológica Hispánica 36.

Huerta, A., Querol, X., Sáez, A., Cabrera, L., 1997. Mineralogy and Geochemistry of the As Pontes lignites (NW Spain): Relation with paleohydrological basin evolution. Migration and Interaction in Sedimentary basins and Orogenic Belts. GEOFLUIDS II'97. Contributions to the Second International Conference on Fluid Evolution. Geological Society Special Publication, pp. 370-373.

Isaaks, E.J., Srivastava, R.M., 1989. An introduction to Applied Geostatistics. Oxford University Press, 561 pp.

Jones, T.A., 1988. Geostatistical Models with Stratigraphic Control - Short Note. Computers & Geosciences 14, 135-138.

Jones, T.J., Hamilton, D.E., Johnson, C.R., 1986. Contouring geologic surfaces with the computer. Van Nostrand Reinhold, New York.

Journel, A., 1986. Geostatistics: Models and Tools for the Earth Sciences. Mathematical Geology 18, 119-140.

Journel, A., Kyriakidis, P.C., Mao, S., 2000. Correcting the Smoothing Effect of Estimators: A Spectral Postprocessor. Mathematical Geology 32, 787-813.

Journel, A.G., 1983. Nonparametric Estimation of Spatial Distributions. Mathematical Geology 15, 445-468.

Journel, A.G., Huijbregts, C.J., 1978. Mining geostatistics. Academic Press, 600 pp.

Journel, A.G., Rossi, M., 1989. When do we need a trend in kriging? Mathematical Geology 21, 715-739.

Kane, V.E., Begovich, C.L., Butz, T.R., Myers, D.E., 1982. Interpretation of Regional Geochemistry Using Optimal Interpolation Parameters. Computers & Geosciences 8, 117-135.

Kupfersberger, H., Deutsch, C.V., 1999. Methodology for Integrating Analog Geologic Data in 3-D Variogram Modeling. American Association of Petroleum Geologists Bulletin 83, 1262-1278.

Langlais, V., Doyle, J.D., Sweet, M.L., Geehan, G., 1993. An additional geological input to SIS: the vertical organization of lithofacies, in: Eschard, R., Doliguez, B. (Eds.), Subsurface Reservoir Characterization from Outcrop Observations. Editions Technip, Paris, pp. 111-123.

Matheron, G., 1963. Principles of geostatistics. Economic Geology 58, 1246-1266.

Moyeed, R.A., Papritz, A., 2002. An Empirical Comparision of Kriging Methods for Nonlinear Spatial Point Prediction. Mathematical Geology 34, 365-386.

Pebesma, E.J., Wesseling, C.G., 1998. GSTAT: A program for geostatistical modelling, prediction and simulation. Computers & Geosciences 24, 17-31.

Rouhani, S., 1986. Comparative study of ground-water mapping techniques. Ground Water 24, 207-216.

Sáez, A., Cabrera, L., 2002. Sedimentological and paleohydrological responses to tectonics and climate in a small, closed, lacustrine system: Oligocene As Pontes Basin (Spain). Sedimentology 49, 1073-1094.

Santanach, P., Baltuille, J.M., Cabrera, L., Monge, C., Sáez, A., Vidal-Romaní, J.R., 1988. Cuencas terciarias gallegas relacionadas con corredores de fallas direccionales, Simposio sobre: Aportación al Programa Internacional de Correlación Geológica. Sociedad Geologica de España, pp. 123-133.

Santanach, P., Ferrús, B., Cabrera, L., Sáez, A., 2005. Origin of a restraining bend in an evolving strike-slip system: The Cenozoic As Pontes basin (NW Spain). Geologica Acta 3, 225-239.

Schuenemeyer, J.H., Power, H., 2000. Uncertainty estimation for resource assessment - an application to coal. Mathematical Geology 32, 521-541.

Starks, T.H., Behrens, N.A., Fang, J.H., 1982. The combination of sampling and kriging in the regional estimation of coal resources. Mathematical Geology 14, 87-106.

Teegavarapu, R.S.V., Chandramouli, V., 2005. Improved weighting methods, deterministic and stochastic data-driven models for estimation of missing precipitation records. Journal of Hydrology 312, 191-206.

Tercan, A.E., Karayigit, A.I., 2001. Estimation of lignite reserve in the Kalburcayiri field, Kangal basin, Sivas, Turkey. International Journal of Coal Geology 47, 91-100.

Turner, B.R., Richardson, D., 2004. Geological controls on the sulphur content of coal seams in the Northumberland Coalfield, Northeast England. International Journal of Coal Geology 60, 169-196.

Watson, W.D., Ruppert, L.F., Bragg, L.J., Tewalt, S.J., 2001. A geostatistical approach to predicting sulfur content in the Pittsburgh coal bed. International Journal of Coal Geology 48, 1-22.

Weber, D.D., Englund, E.J., 1992. Evaluation and comparison of spatial interpolators. Mathematical Geology 24, 381-391.

Weber, D.D., Englund, E.J., 1994. Evaluation and comparision of spatial interpolators II. Mathematical Geology 26, 589-603.

Yamamoto, J.K., 2005. Correcting the Smoothing Effect og Ordinary Kriging Estimates. Mathematical Geology 37, 69-94.

Zimmerman, D., Pavlik, C., Ruggles, A., Armstrong, P., 1999. An experimental comparision of ordinary and universal kriging and inverse distance weighting. Mathematical Geology 31, 375-390.

Zoraster, S., 1996. Imposing Geologic Interpretarions on Computer-Generated Contours Using Distance Transformation. Mathematical Geology 28, 969-985.

Figure Captions

Figure 1. Geological setting and characteristics of the As Pontes basin. **(A)** Location of the As Pontes basin. **(B)** Geological map of the basin showing the main tectonic structures that affect the basement. Note the strike-slip fault and associated thrusts, which bound the northern basin margin; the N–S oriented normal faults and the E–W and NE–SW oriented thrusts. **(C)** Longitudinal sketch of the basin showing the main stratigraphic units, sedimentary facies and basement structures (see arrows for location on 1B), notice the stratigraphic position of the 6AW coal zone. **(D)** Paleogeographic sketches of the basin during deposition of the 6A interval.

Figure 2. Well location in the studied part of 6AW zone. Location of the NW-SE reference section that is used as an example in Figures 4, 12, 15, 18, 21 and 22 is shown. Coordinates in the lower left frame are in kilometres. See Figure 1B and 1D for structural details.

Figure 3. Relative frequency of calorific values **(A)** and sulfur percentages **(B)** in the three major coal facies in the 6AW coal seam zone. Plotted information corresponds to the core data upscaled to the size of grid cells. These were computed biased to the facies logs and assuming a geological layering (see section 5.1). Upscaled data (see section 3.3) are close to the original because of the fine grid used. Original data consisted in more than 2500 analyses (513 in PBC, 1840 in DBC, and 227 in XBC) for each property.

Figure 4. Reference section showing the different grid layering styles used for facies interpolations. See location of the section in Figure 2. Note that only one tenth of the grid layers is shown as reference. Vertical exaggeration 10x.

Figure 5. Standardized variograms for the transformed Gaussian property. Grey dots and dashed curves correspond to the experimental variograms derived from upscaled well data. No significant differences were observed in the experimental variograms derived from the four different grid layering styles. Continuous curves correspond to the theoretical model fitted (Hr and Vr stands for horizontal and vertical variogram ranges respectively):

$\gamma(h) = 0.6 \cdot \text{Exp}\ (Hr = 500m, Vr = 1.4m) + 0.4 \cdot \text{Exp}\ (Hr = 100m, Vr = 3m)$.

Figure 6. Areal trend derived from the interpolation of averaged values of the continuous property values along each well. The different shades reflect the average facies along each well. A clear non-stationary facies distribution is shown. Higher values are located predominantly near the basin margins (specially in the northern) where facies AM dominates. Intermediate-low values occur in the centre of the coal zone where facies DBC dominates. The lower values are restricted to some zones with dominance of facies PBC and LM.

Figure 7. Standardized variograms for the residual of the transformed continuous Gaussian property. Grey dots and dashed curves correspond to the experimental variograms derived from upscaled well data. No significant differences were observed in the experimental variograms derived from the four different layering styles.

Continuous curves correspond to the theoretical model fitted (Hr and Vr stands for horizontal and vertical variogram ranges respectively):
γ (h) = 0.6·Exp (Hr = 400m, Vr = 1.4m) + 0.4·Exp (Hr= 100m, Vr =3m).

Figure 8. Non-standardized indicator variograms assuming a geological layering. Grey dots and dashed curves correspond to the experimental variograms derived from upscaled well data. No significant differences were observed in the experimental variograms derived from the four different layering styles. Continuous curves correspond to the theoretical models fitted (Hr and Vr stands for horizontal and vertical variogram ranges respectively):
γ (h) LM = 0.018·Exp (Hr = 500m, Vr = 1.4m) + 0.012·Exp (Hr = 100m, Vr =3m).
γ (h) PBC = 0.063·Exp (Hr = 200m, Vr = 1.4m) + 0.042·Exp (Hr = 100m, Vr =3m).
γ (h) DBC = 0.150·Exp (Hr = 500m, Vr = 1.4m) + 0.100·Exp (Hr = 100m, Vr =3m).
γ (h) XBC = 0.039·Exp (Hr = 300m, Vr = 1.4m) + 0.026·Exp (Hr = 100m, Vr =3m).
γ (h) AM = 0.113·Exp (Hr = 700m, Vr = 1.4m) + 0.076·Exp (Hr = 100m, Vr =3m).

Figure 9. Areal trends for each indicator property derived from the interpolation of averaged values along each well. The maps correspond to the areal proportions of each facies. Note the difference in the range of the greyscale among the different facies.

Figure 10. Standardized variograms for the residual of the indicator properties, assuming a geological layering. Grey dots and dashed curves correspond to the experimental variogram derived from upscaled well data. No significant differences were observed in the experimental variograms derived from the four different layering styles. Continuous curves correspond to the theoretical models fitted (Hr and Vr stands for horizontal and vertical variogram ranges respectively):
γ (h) LM = 0.6·Exp (Hr = 500m, Vr = 1.4m) + 0.4·Exp (Hr = 100m, Vr =3m).
γ (h) PBC = 0.6·Exp (Hr = 200m, Vr = 1.4m) + 0.4·Exp (Hr = 100m, Vr =3m).
γ (h) DBC = 0.6·Exp (Hr = 500m, Vr = 1.4m) + 0.4·Exp (Hr = 100m, Vr =3m).
γ (h) XBC = 0.6·Exp (Hr = 300m, Vr = 1.4m) + 0.4·Exp (Hr = 100m, Vr =3m).
γ (h) AM = 0.6·Exp (Hr = 700m, Vr = 1.4m) + 0.4·Exp (Hr = 100m, Vr =3m).

Figure 11. (A) Relationship between DBC proportion predicted by CV and by the interpolation along the entire grid. Results shown correspond to a geological grid layering style and NN set to 48. **(B)** CV errors and smoothing using randomly generated unconditioned facies estimates, each line corresponds to a different grid layering style and was generated through the linear regression of the results for 100 realizations with varying DBC proportion, correlation factor (R2) was in all cases above 0.99.

Figure 12. Reference section showing facies distribution obtained by using different grid layering styles. In all frames the interpolation method used was indicator kriging with an areal trend (IK-T) and NN set to 48. See location of the section in Figure 2. Arrows indicate the position of intersected wells. Vertical exaggeration 10x.

Figure 13. (A) Relationship between DBC proportion predicted by CV (smoothing effect) and CV error for the different grid layering styles tested. Only results for indicator approach methods and NN set to 48 are shown; results for truncated approach methods are not presented due to their limited performance (section 5.2), intermediate NN (48) provided a good balance between visual results, CV error and smoothing (section 5.2). **(B)** Relationship between smoothing effect, and CV error divided by the

CV error obtained with total smoothing (DBC facies proportion at 100%, i.e. mean mapping).

Figure 14. Relationship between the original upscaled DBC proportion and the CV error using facies estimates with total smoothing (DBC facies proportion at 100%, i.e. Mean mapping) for the different grid layering styles.

Figure 15. Reference section showing facies distribution obtained by using different interpolation methods assuming a geological grid layering style. In all cases NN was set to 48. See location of the section in Figure 2. Arrows indicate the position of intersected wells. Vertical exaggeration 10x.

Figure 16. Relationship between DBC proportion predicted by CV (smoothing effect) and CV error for each interpolation method compared, considering geological (A) and proportional (B) grid layering styles. Results for different NN (4, 12, 24, 48, 96, 192 and 288) are shown.

Figure 17. Relationship between DBC proportion predicted by CV (smoothing effect) and CV error for each interpolation method compared, geological and proportional grid layering styles, and different NN set ups: 12 **(A)**, 48 **(B)** and 192 **(C)**.

Figure 18. Reference section showing facies distribution obtained by changing horizontal variogram ranges. In all frames the interpolation method used was indicator kriging with an areal trend (IK-T) and NN was set to 48. See location of the section in Figure 2. Arrows indicate the position of intersected wells. Vertical exaggeration 10x

Figure 19. Relationship between DBC proportion predicted by cross validation CV (smoothing effect) and CV error for each scenario of horizontal variogram range uncertainty.

Figure 20. Fence diagrams viewed from the S showing 3D reconstructions of the 6AW zone. **(A)** Facies reconstruction using IK-T (NN set to 48 and a geological grid layering style). **(B)** Interpolation of calorific values using the facies distribution as a template. **(C)** Interpolation of total sulphur percentages using the facies distribution as a template. Vertical exaggeration 10x. See Figure 21 and 22, and supplementary material for further detail.

Figure 21. Reference section showing calorific value interpolations without using facies distribution as a template **(A)** and using facies distribution as a template **(B)**. See location of the section in Figure 2. Arrows indicate the position of intersected wells. Vertical exaggeration 10x.

Figure 22. Reference section showing total sulphur percentage interpolations without using facies distribution as a template **(A)** and using facies distribution as a template **(B)**. See location of the section in Figure 2. Arrows indicate the position of intersected wells. Vertical exaggeration 10x.

Table Captions

Table 1: Classification of the interpolation methods compared. This classification is based on the approach to deal with the categorical property, the weighting criteria and the inclusion of trends.

Table 2: Cross validation results for calorific value (dry basis) **(a)** and total sulphur percentage (dry basis) **(b)**. See text for related discussion

Supplementary Material

Facies_IK-T_Geo_NN48.wrl file: virtual reality file with 3D view in Figure 20A

PCAdb_using facies.vrl file: virtual reality file with 3D view in Figure 20B

SULdb_using facies.wrl: virtual reality file with 3D view in Figure 20C

corvrml.exe file: executable file with the Cortona VRML Client (by Parallel Graphics©) for navigating .vrl files with Internet Explorer

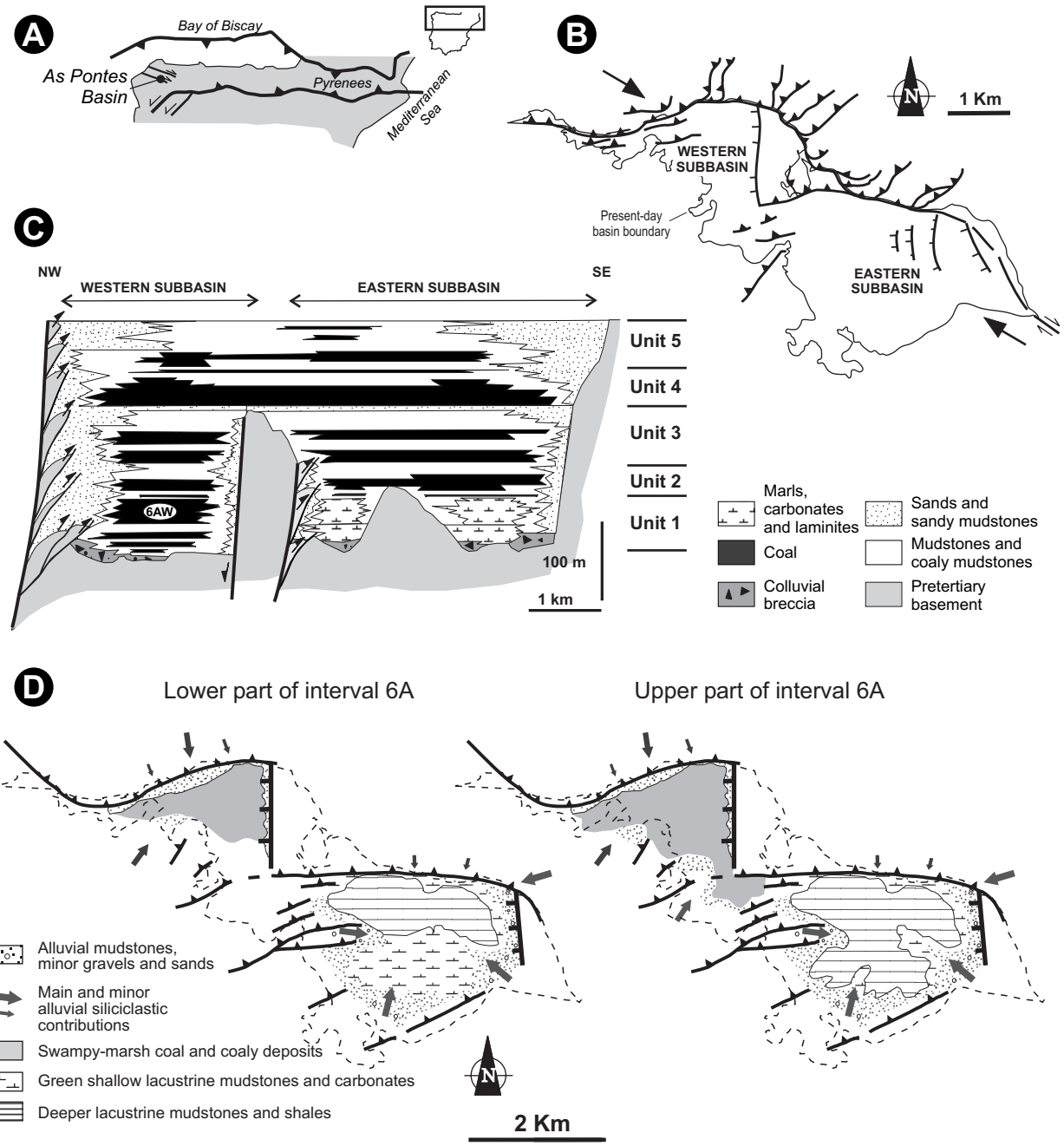

Figure 1. Geological setting and characteristics of the As Pontes basin. **(A)** Location of the As Pontes basin. **(B)** Geological map of the basin showing the main tectonic structures that affect the basement. Note the strike-slip fault and associated thrusts, which bound the northern basin margin; the N–S oriented normal faults and the E–W and NE–SW oriented thrusts. **(C)** Longitudinal sketch of the basin showing the main stratigraphic units, sedimentary facies and basement structures (see arrows for location on 1B), notice the stratigraphic position of the 6AWcoal zone. **(D)** Paleogeographic sketches of the basin during deposition of the 6A interval.

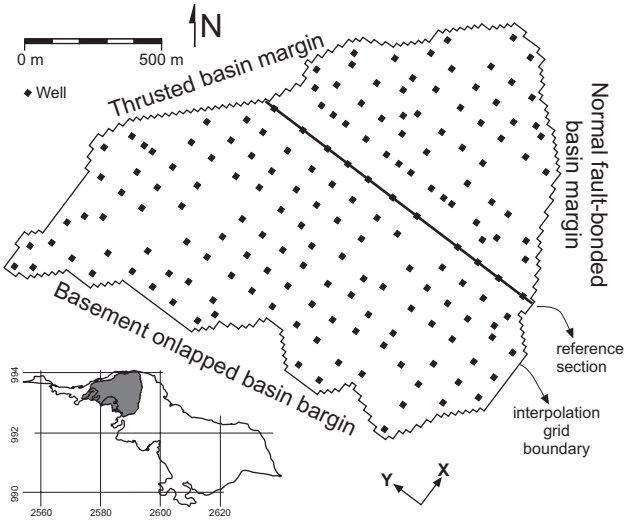

Figure 2. Well location in the studied part of 6AW zone. Location of the NW-SE reference section that is used as an example in Figures 4, 12, 15, 18, 21 and 22 is shown. Coordinates in the lower left frame are in kilometres. See Figure 1B and 1D for structural details.

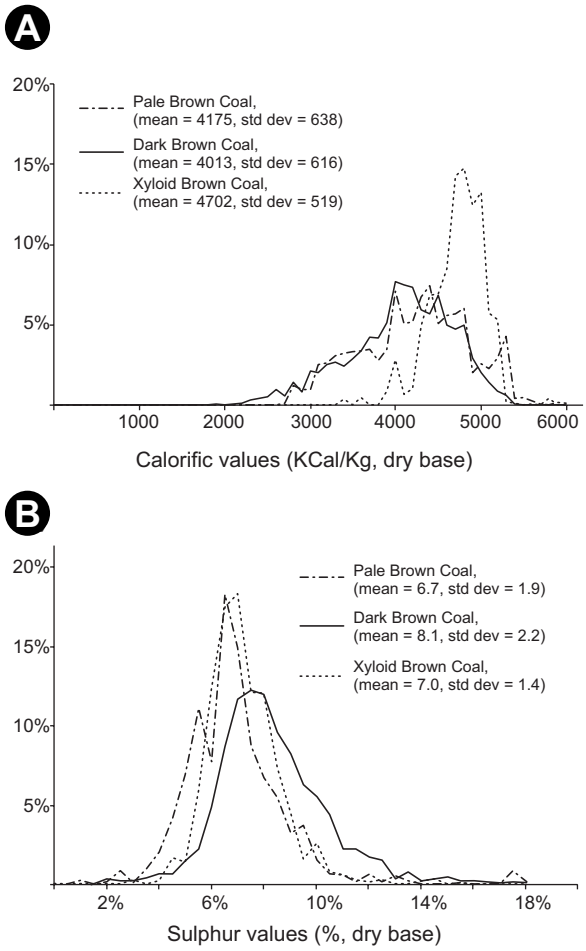

Figure 3. Relative frequency of calorific values **(A)** and sulfur percentages **(B)** in the three major coal facies in the 6AW coal seam zone. Plotted information corresponds to the core data upscaled to the size of grid cells. These were computed biased to the facies logs and assuming a geological layering (see section 5.1). Upscaled data (see section 3.3) are close to the original because of the fine grid used. Original data consisted in more than 2500 analyses (513 in PBC, 1840 in DBC, and 227 in XBC) for each property.

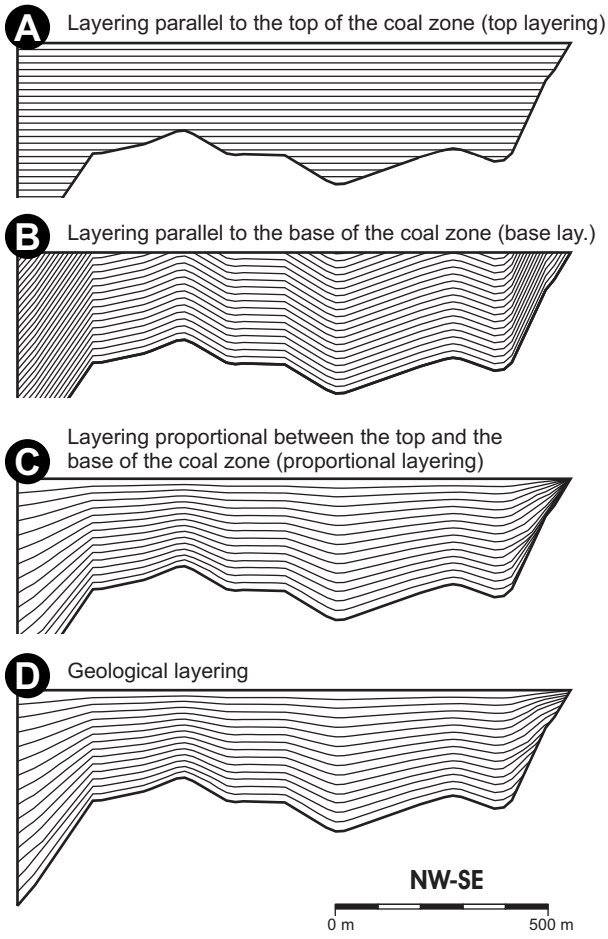

Figure 4. Reference section showing the different grid layering styles used for facies interpolations. See location of the section in Figure 2. Note that only one tenth of the grid layers is shown as reference. Vertical exaggeration 10x

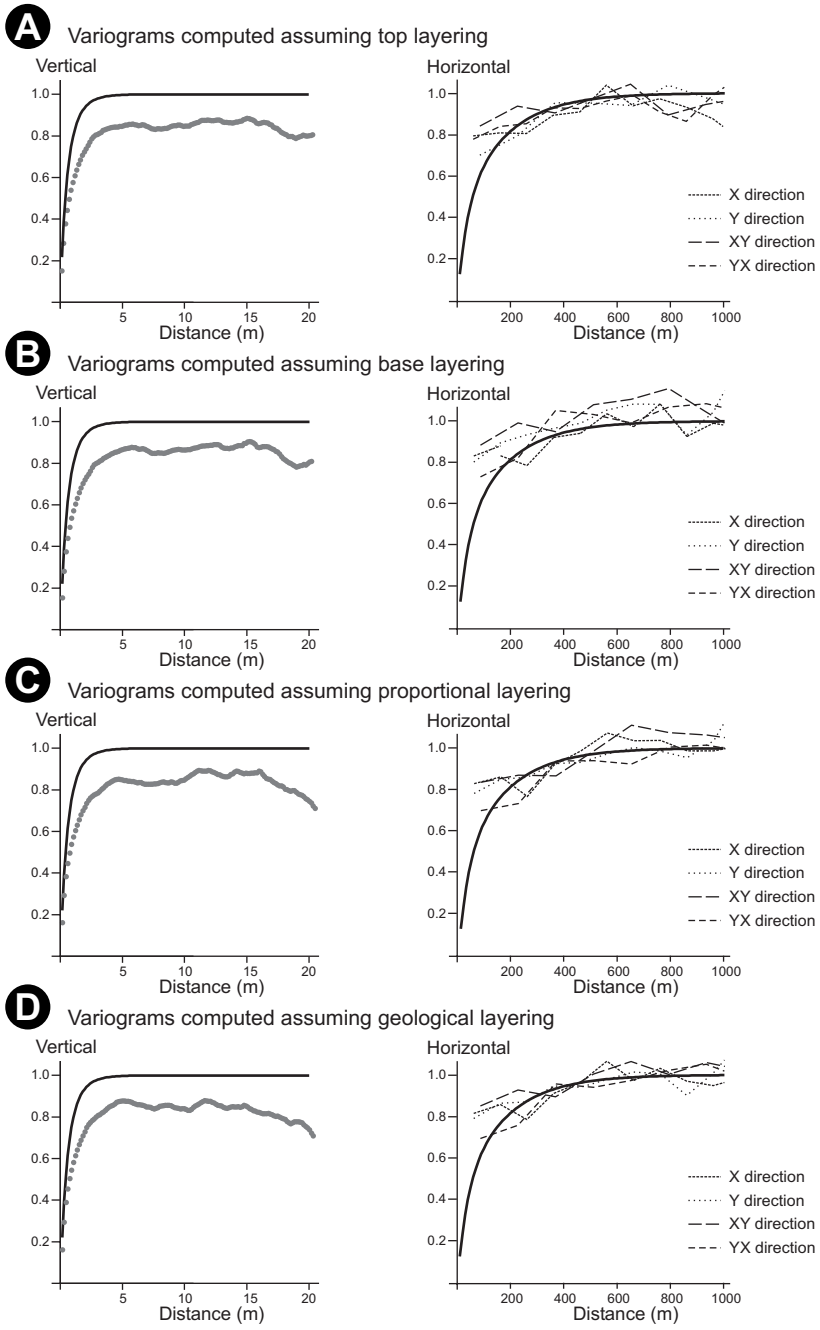

Figure 5: Standardized variograms for the transformed Gaussian property. Grey dots and dashed curves correspond to the experimental variograms derived from upscaled well data. No significant differences were observed in the experimental variograms derived from the four different grid layering styles. Continuous curves correspond to the theoretical model fitted (Hr and Vr stands for horizontal and vertical variogram ranges respectively):

$\gamma(h) = 0.6 \cdot \mathrm{Exp}\,(\mathrm{Hr} = 500\mathrm{m}, \mathrm{Vr} = 1.4\mathrm{m}) + 0.4 \cdot \mathrm{Exp}\,(\mathrm{Hr} = 100\mathrm{m}, \mathrm{Vr} = 3\mathrm{m})$.

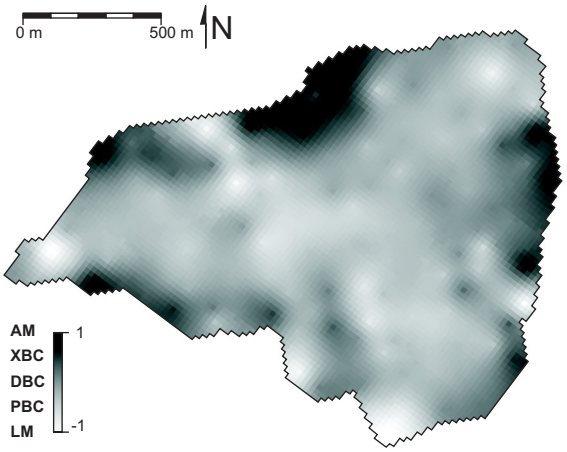

Figure 6. Areal trend derived from the interpolation of averaged values of the continuous property values along each well. The different shades reflect the average facies along each well. A clear non-stationary facies distribution is shown. Higher values are located predominantly near the basin margins (specially in the northern) where facies AM dominates. Intermediate-low values occur in the centre of the coal zone where facies DBC dominates. The lower values are restricted to some zones with dominance of facies PBC and LM.

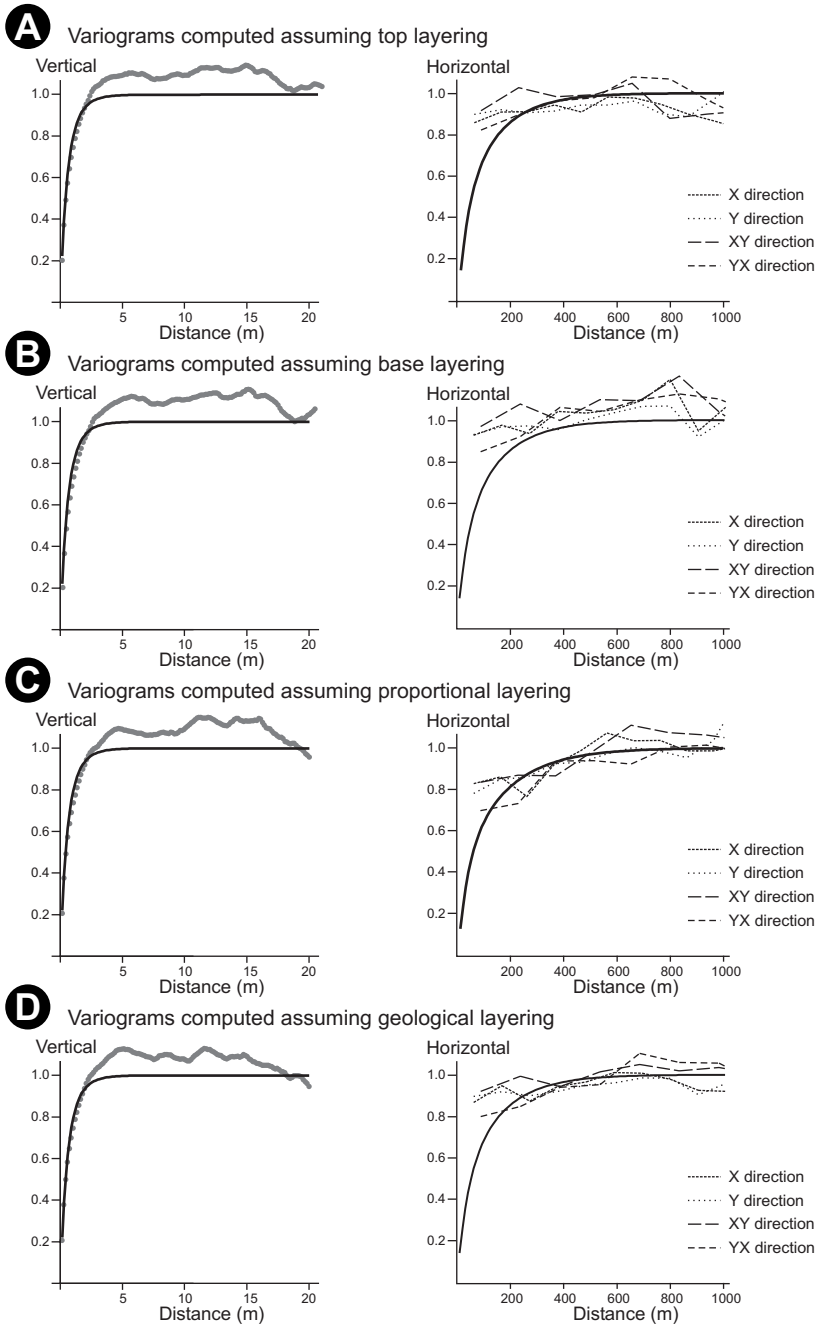

Figure 7: Standardized variograms for the residual of the transformed continuous Gaussian property. Grey dots and dashed curves correspond to the experimental variograms derived from upscaled well data. No significant differences were observed in the experimental variograms derived from the four different layering styles. Continuous curves correspond to the theoretical model fitted (Hr and Vr stands for horizontal and vertical variogram ranges respectively):

$\gamma(h) = 0.6 \cdot \mathrm{Exp}\,(\mathrm{Hr} = 400\mathrm{m}, \mathrm{Vr} = 1.4\mathrm{m}) + 0.4 \cdot \mathrm{Exp}\,(\mathrm{Hr} = 100\mathrm{m}, \mathrm{Vr} = 3\mathrm{m})$.

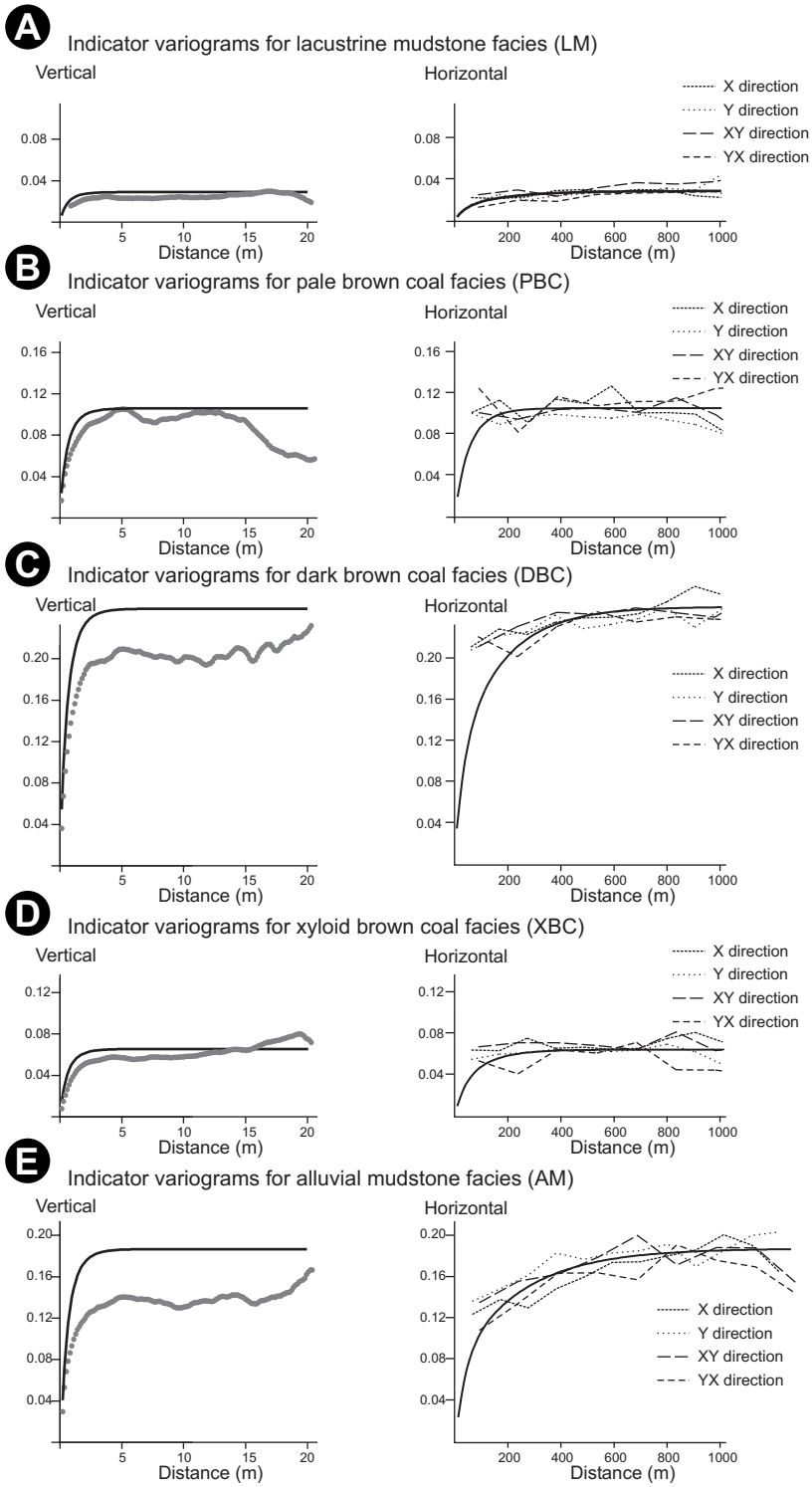

Figure 8: Non-standardized indicator variograms assuming a geological layering. Grey dots and dashed curves correspond to the experimental variograms derived from upscaled well data. No significant differences were observed in the experimental variograms derived from the four different layering styles. Continuous curves correspond to the theoretical models fitted (Hr and Vr stands for horizontal and vertical variogram ranges respectively):

$\gamma(h)\,LM = 0.018 \cdot Exp\,(Hr = 500m, Vr = 1.4m) + 0.012 \cdot Exp\,(Hr = 100m, Vr = 3m).$

$\gamma(h)\,PBC = 0.063 \cdot Exp\,(Hr = 200m, Vr = 1.4m) + 0.042 \cdot Exp\,(Hr = 100m, Vr = 3m).$

$\gamma(h)\,DBC = 0.150 \cdot Exp\,(Hr = 500m, Vr = 1.4m) + 0.100 \cdot Exp\,(Hr = 100m, Vr = 3m).$

$\gamma(h)\,XBC = 0.039 \cdot Exp\,(Hr = 300m, Vr = 1.4m) + 0.026 \cdot Exp\,(Hr = 100m, Vr = 3m).$

$\gamma(h)\,AM = 0.113 \cdot Exp\,(Hr = 700m, Vr = 1.4m) + 0.076 \cdot Exp\,(Hr = 100m, Vr = 3m).$

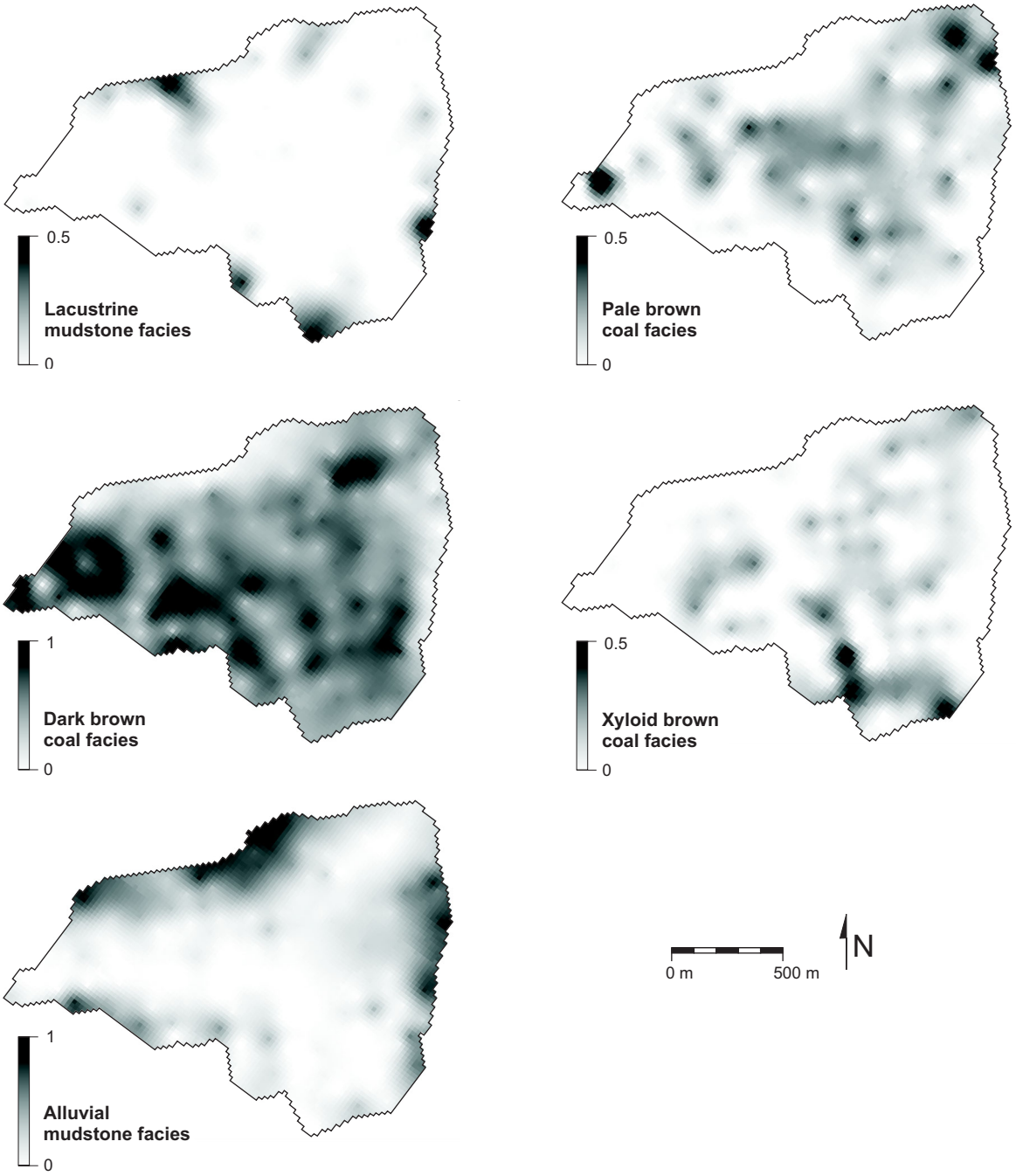

Figure 9. Areal trends for each indicator property derived from the interpolation of averaged values along each well. The maps correspond to the areal proportions of each facies. Note the difference in the range of the greyscale among the different facies.

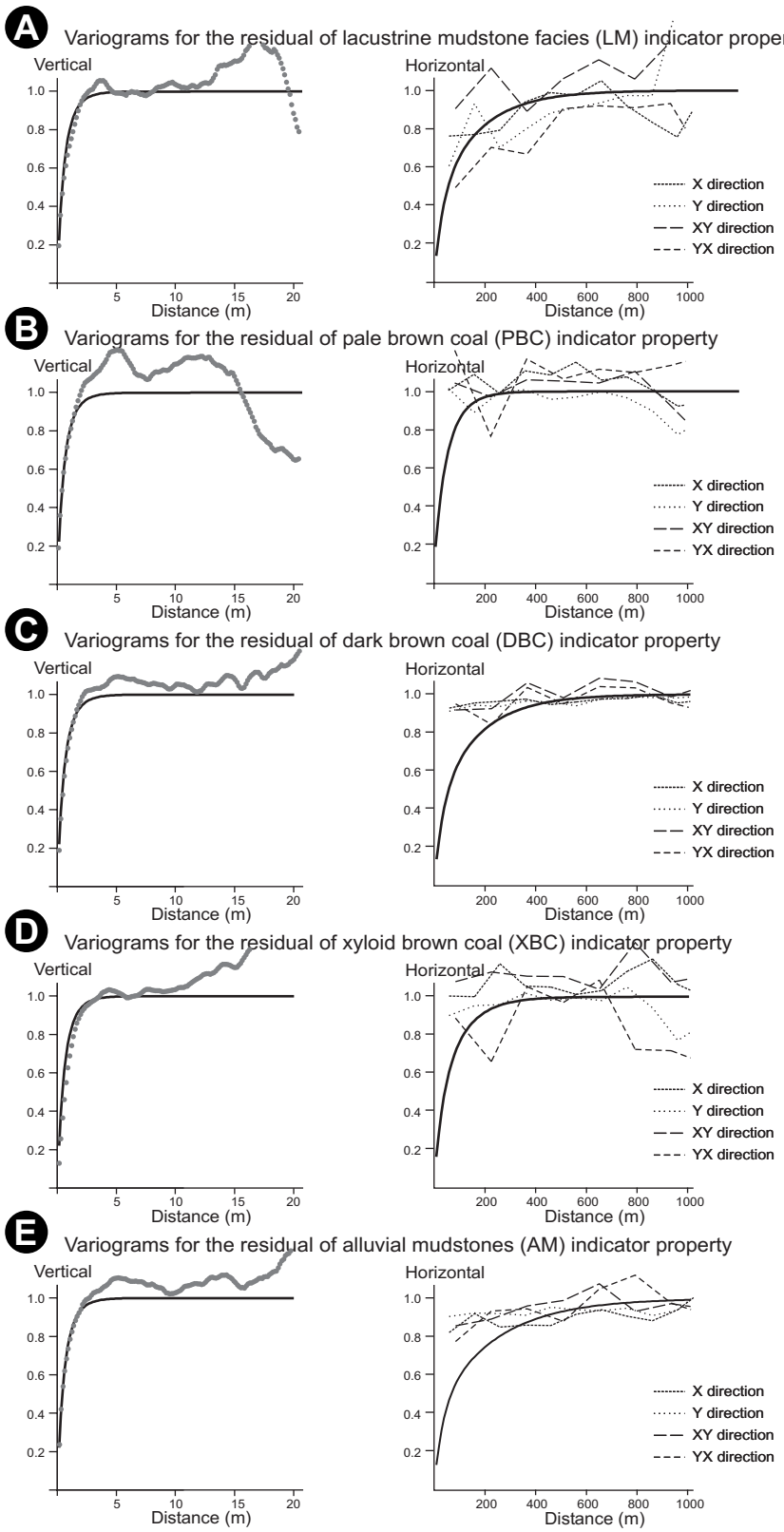

Figure 10: Standardized variograms for the residual of the indicator properties, assuming a geological layering. Grey dots and dashed curves correspond to the experimental variogram derived from upscaled well data. No significant differences were observed in the experimental variograms derived from the four different layering styles. Continuous curves correspond to the theoretical models fitted (Hr and Vr stands for horizontal and vertical variogram ranges respectively):

$\gamma(h)\,\mathrm{LM} = 0.6\cdot\mathrm{Exp}(\mathrm{Hr}=500\mathrm{m}, \mathrm{Vr}=1.4\mathrm{m}) + 0.4\cdot\mathrm{Exp}(\mathrm{Hr}=100\mathrm{m}, \mathrm{Vr}=3\mathrm{m}).$

$\gamma(h)\,\mathrm{PBC} = 0.6\cdot\mathrm{Exp}(\mathrm{Hr}=200\mathrm{m}, \mathrm{Vr}=1.4\mathrm{m}) + 0.4\cdot\mathrm{Exp}(\mathrm{Hr}=100\mathrm{m}, \mathrm{Vr}=3\mathrm{m}).$

$\gamma(h)\,\mathrm{DBC} = 0.6\cdot\mathrm{Exp}(\mathrm{Hr}=500\mathrm{m}, \mathrm{Vr}=1.4\mathrm{m}) + 0.4\cdot\mathrm{Exp}(\mathrm{Hr}=100\mathrm{m}, \mathrm{Vr}=3\mathrm{m}).$

$\gamma(h)\,\mathrm{XBC} = 0.6\cdot\mathrm{Exp}(\mathrm{Hr}=300\mathrm{m}, \mathrm{Vr}=1.4\mathrm{m}) + 0.4\cdot\mathrm{Exp}(\mathrm{Hr}=100\mathrm{m}, \mathrm{Vr}=3\mathrm{m}).$

$\gamma(h)\,\mathrm{AM} = 0.6\cdot\mathrm{Exp}(\mathrm{Hr}=700\mathrm{m}, \mathrm{Vr}=1.4\mathrm{m}) + 0.4\cdot\mathrm{Exp}(\mathrm{Hr}=100\mathrm{m}, \mathrm{Vr}=3\mathrm{m}).$

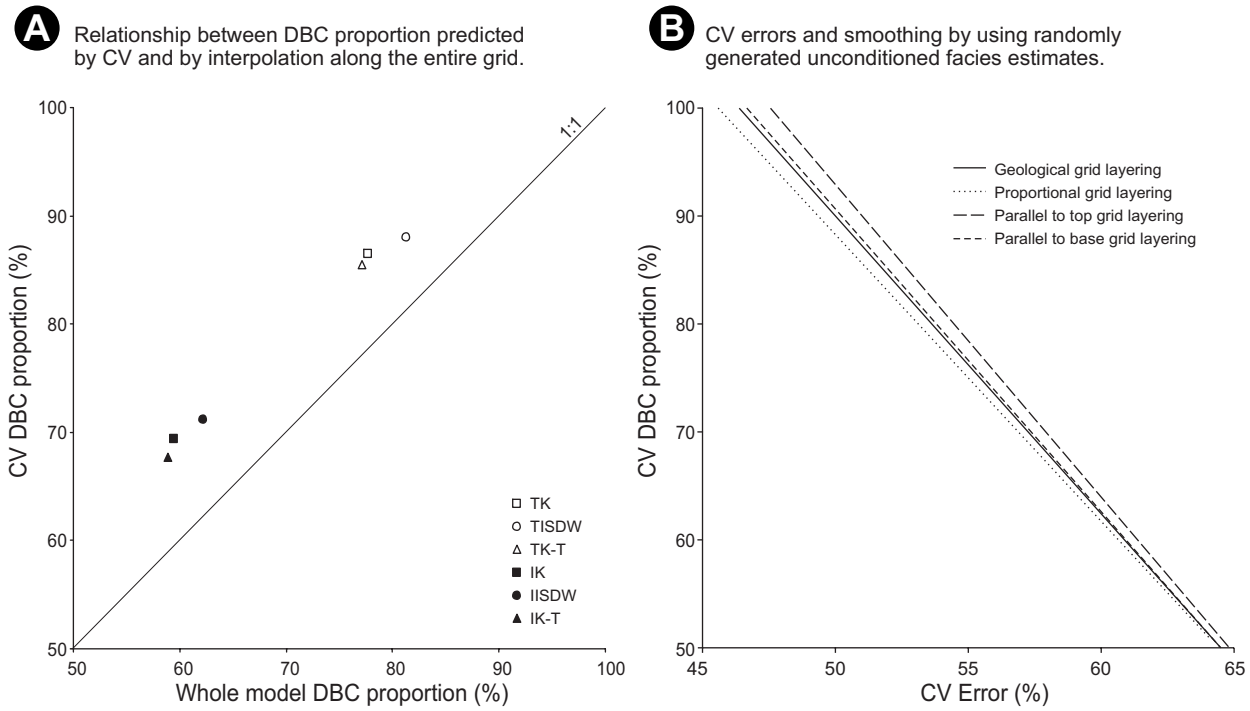

Figure 11. (A) Relationship between DBC proportion predicted by CV and by the interpolation along the entire grid. Results shown correspond to a geological grid layering style and NN set to 48. (**B)** CV errors and smoothing using randomly generated unconditioned facies estimates, each line corresponds to a different grid layering style and was generated through the linear regression of the results for 100 realizations with varying DBC proportion, correlation factor (R^2) was in all cases above 0.99.

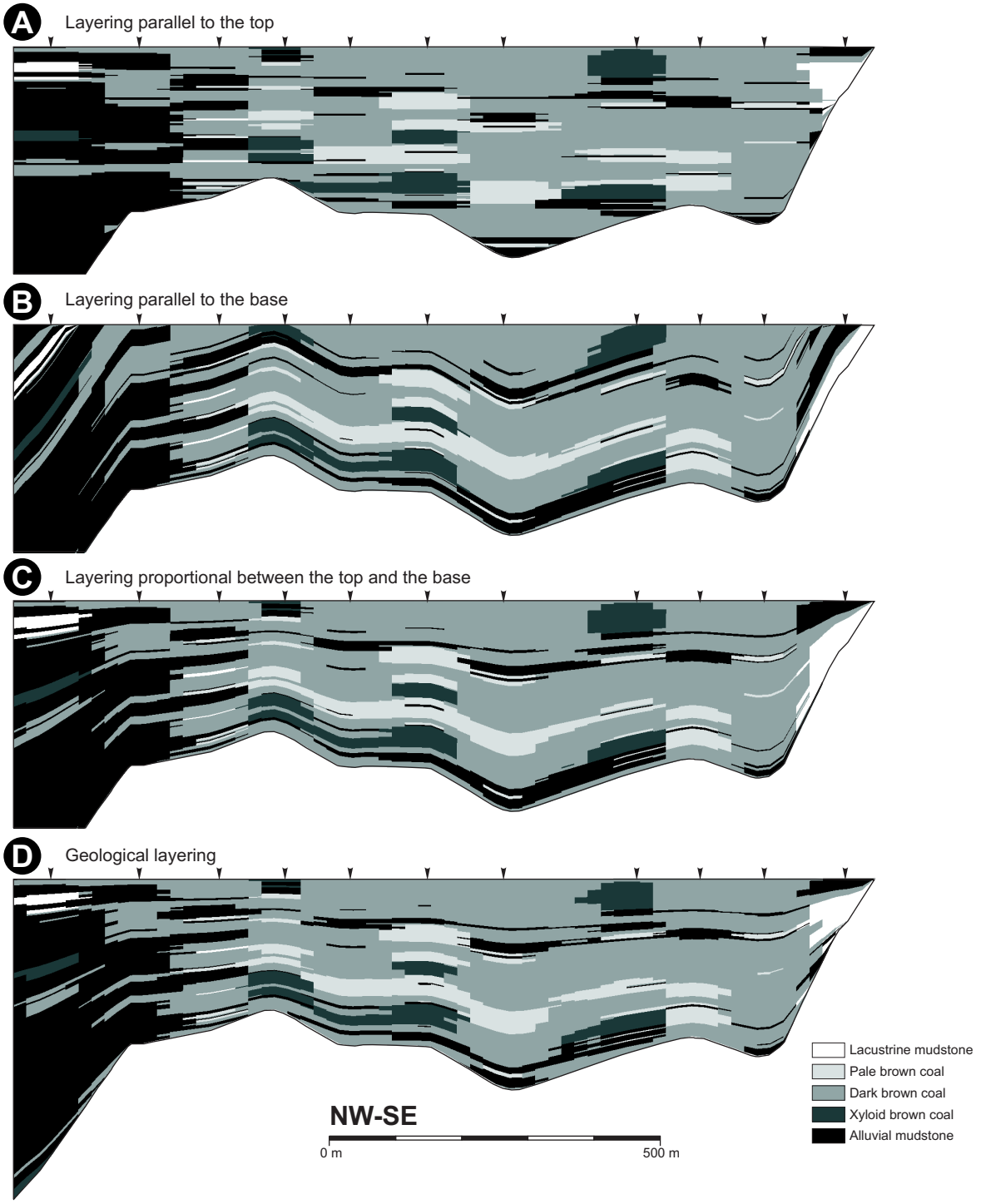

Figure 12: Reference section showing facies distribution obtained by using different grid layering styles. In all frames the interpolation method used was indicator kriging with an areal trend (IK-T) and NN set to 48. See location of the section in Figure 2. Arrows indicate the position of intersected wells. Vertical exaggeration 10x

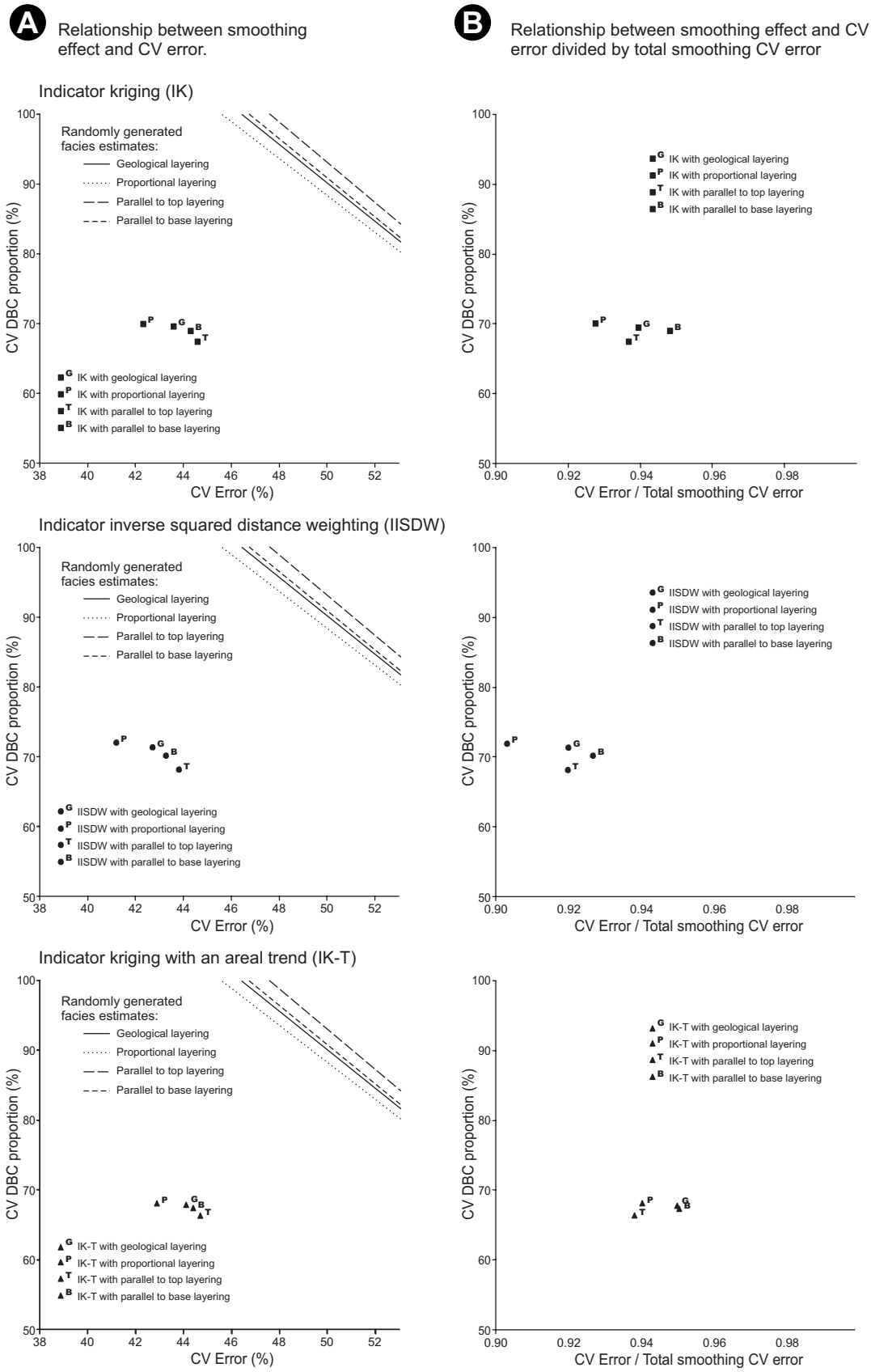

Figure 13. (A) Relationship between DBC proportion predicted by CV (smoothing effect) and CV error for the different grid layering styles tested. Only results for indicator approach methods and NN set to 48 are shown; results for truncated approach methods are not presented due to their limited performance (section 5.2), intermediate NN (48) provided a good balance between visual results, CV error and smoothing (section 5.2). **(B)** Relationship between smoothing effect, and CV error divided by the CV error obtained with total smoothing (DBC facies proportion at 100%, i.e. mean mapping).

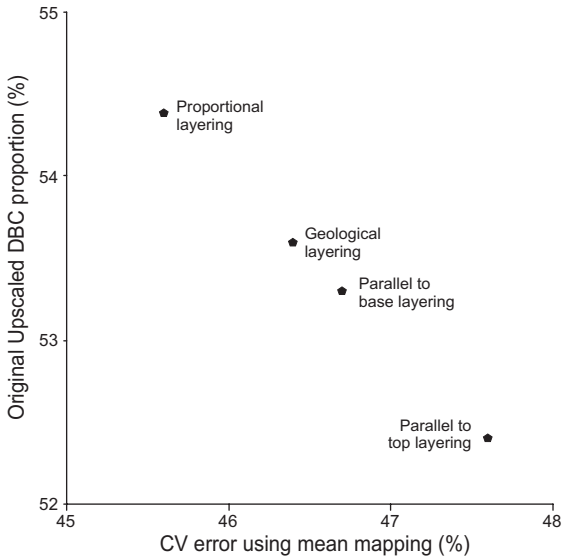

Figure 14. Relationship between the original upscaled DBC proportion and the CV error using facies estimates with total smoothing (DBC facies proportion at 100%, i.e. Mean mapping) for the different grid layering styles.

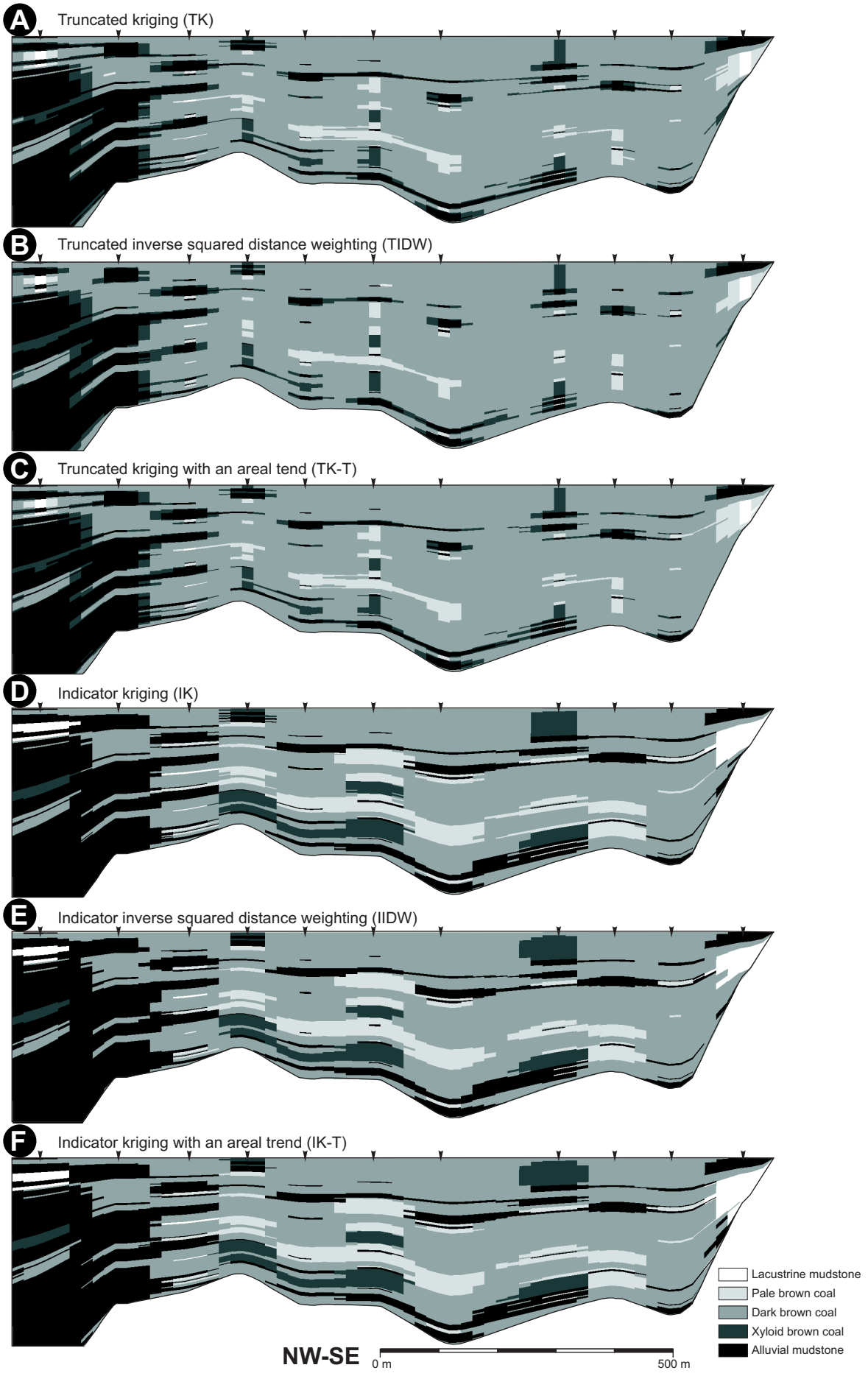

Figure 15: Reference section showing facies distribution obtained by using different interpolation methods assuming a geological grid layering style. In all cases NN was set to 48. See location of the section in Figure 2. Arrows indicate the position of intersected wells. Vertical exaggeration 10x.

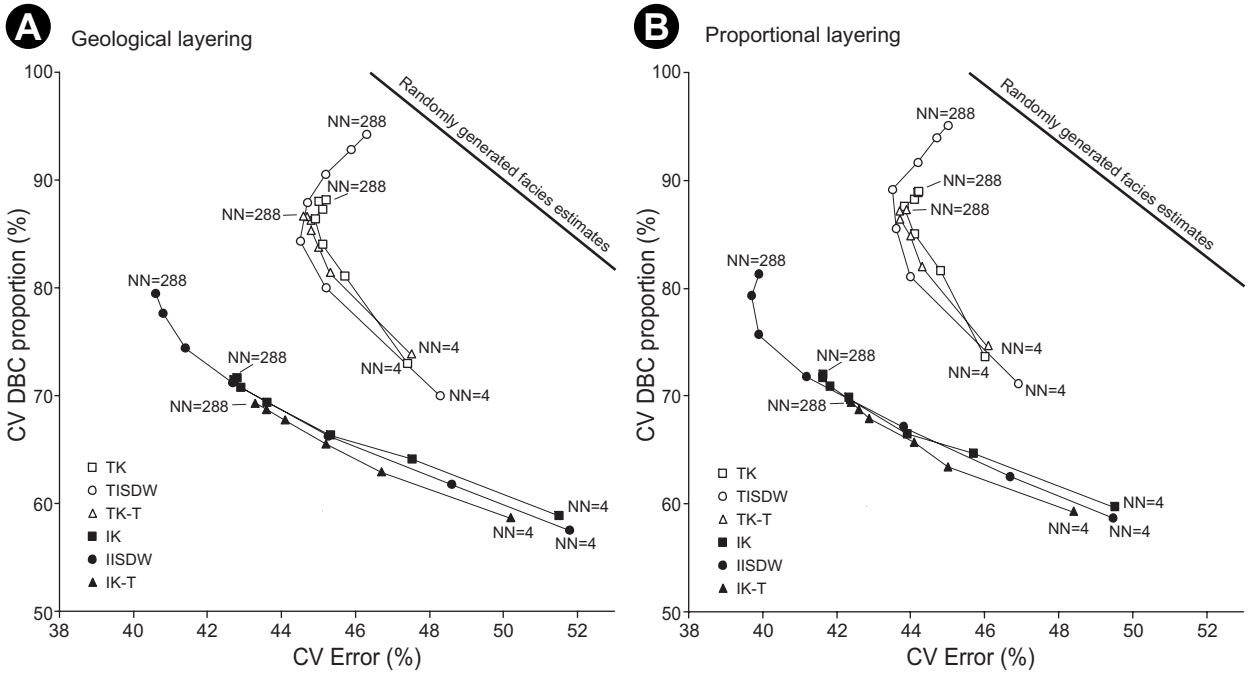

Figure 16. Relationship between DBC proportion predicted by CV (smoothing effect) and CV error for each interpolation method compared, considering geological **(A)** and proportional **(B)** grid layering styles. Results for different NN (4, 12, 24, 48, 96, 192 and 288) are shown.

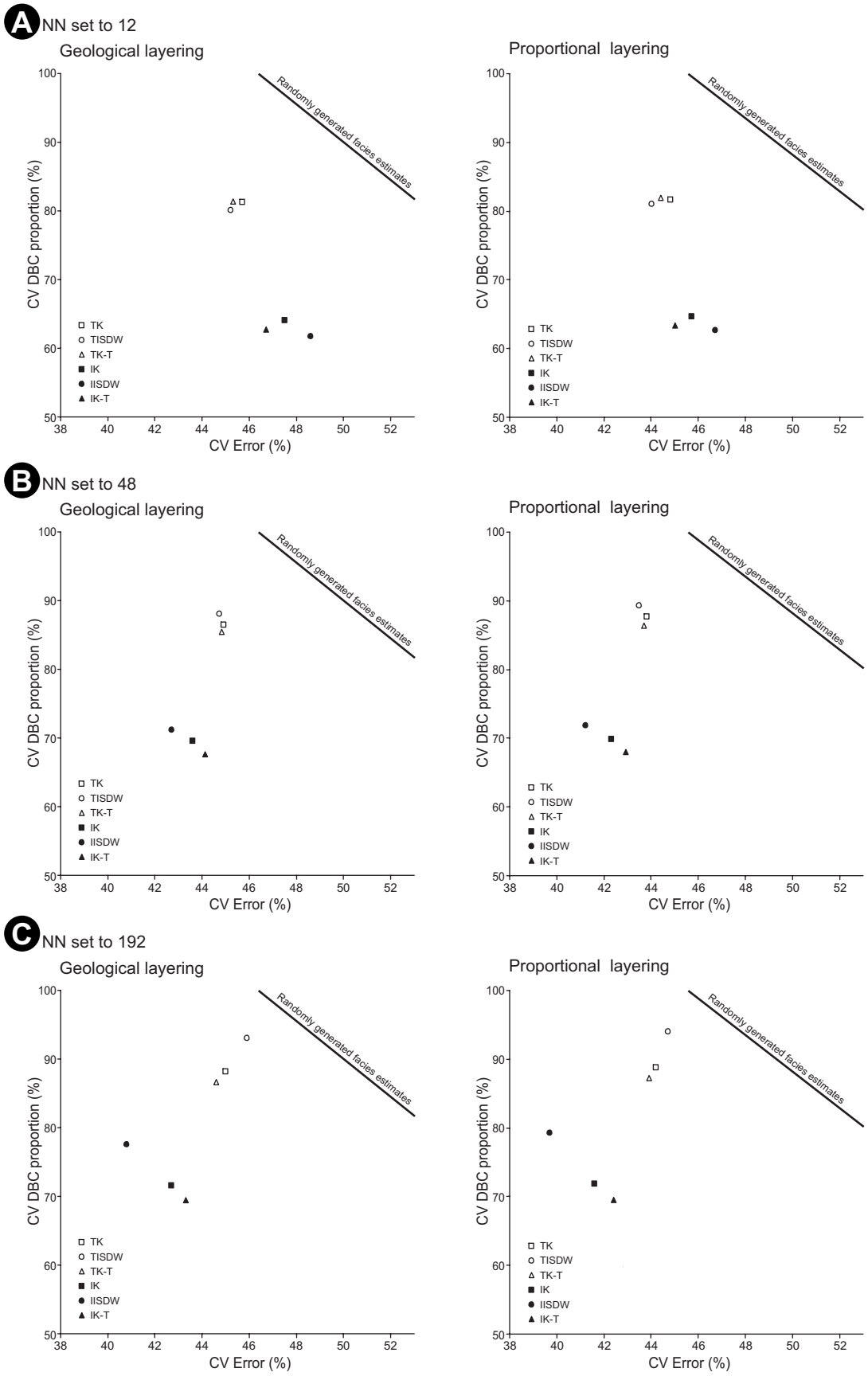

Figure 17. Relationship between DBC proportion predicted by CV (smoothing effect) and CV error for each interpolation method compared, geological and proportional grid layering styles, and different NN set ups: 12 **(A)**, 48 **(B)** and 192 **(C)**.

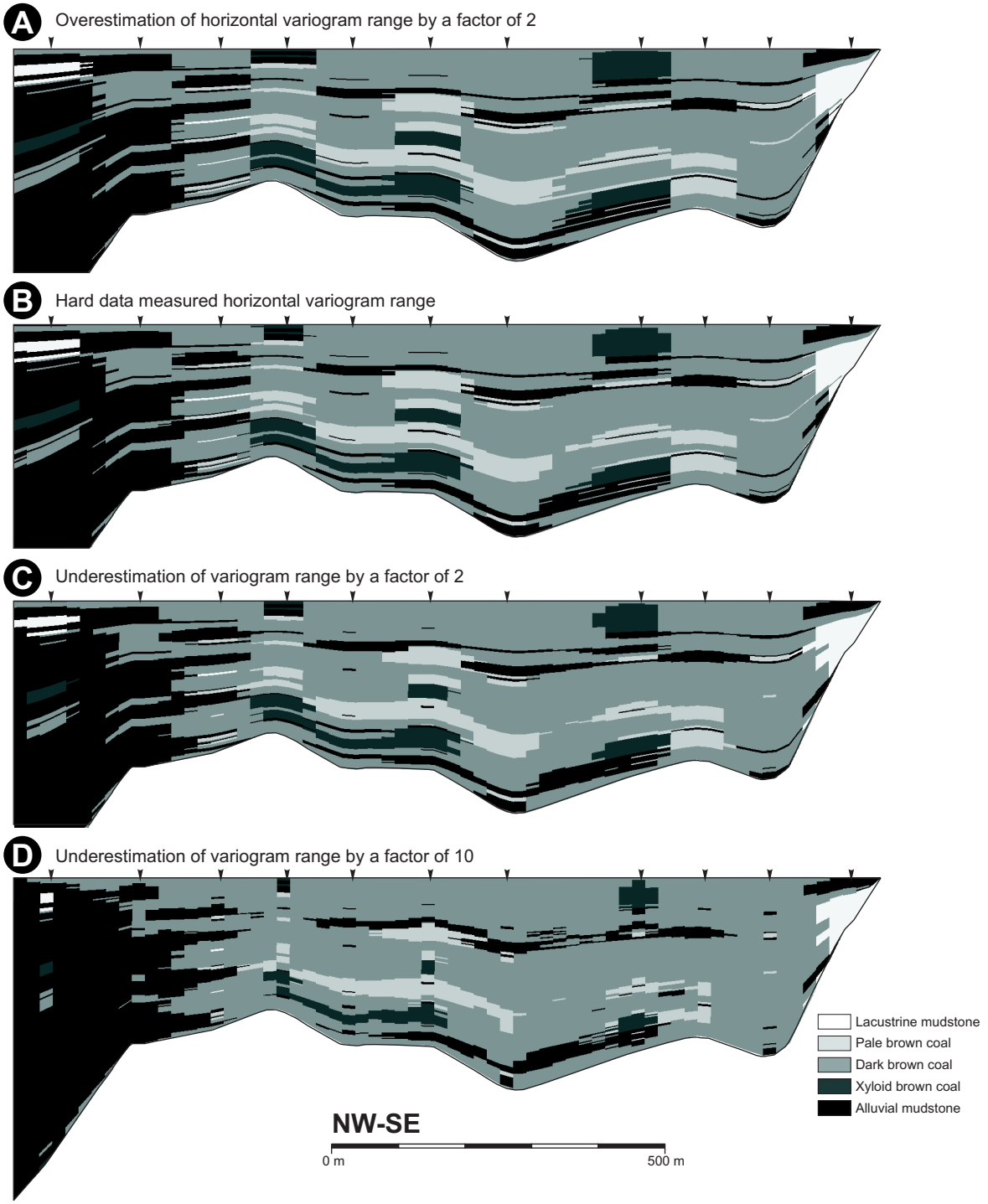

Figure 18: Reference section showing facies distribution obtained by changing horizontal variogram ranges. In all frames the interpolation method used was indicator kriging with an areal trend (IK-T) and NN was set to 48. See location of the section in Figure 2. Arrows indicate the position of intersected wells. Vertical exaggeration 10x

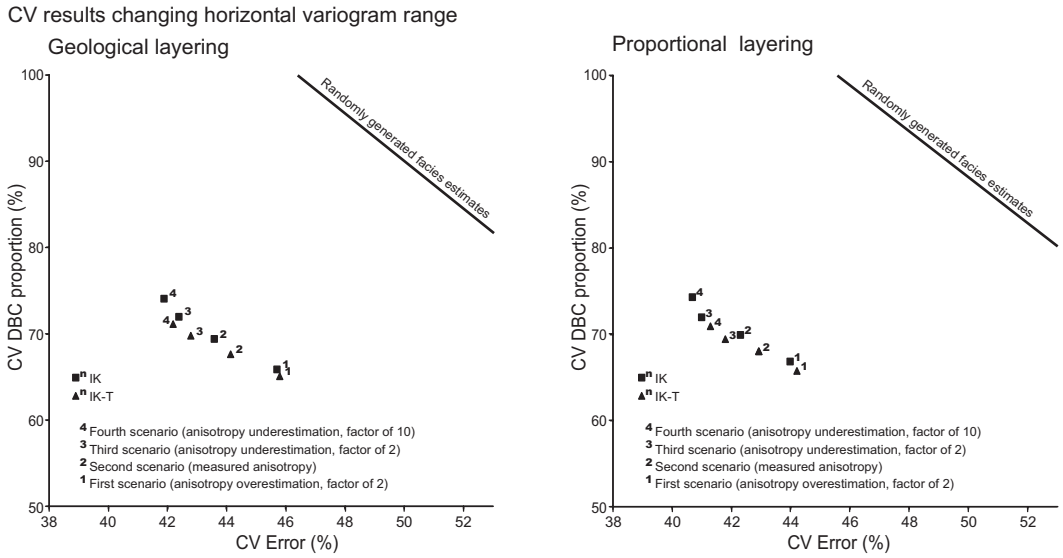

Figure 19. Relationship between DBC proportion predicted by cross validation CV (smoothing effect) and CV error for each scenario of horizontal variogram range uncertainty.

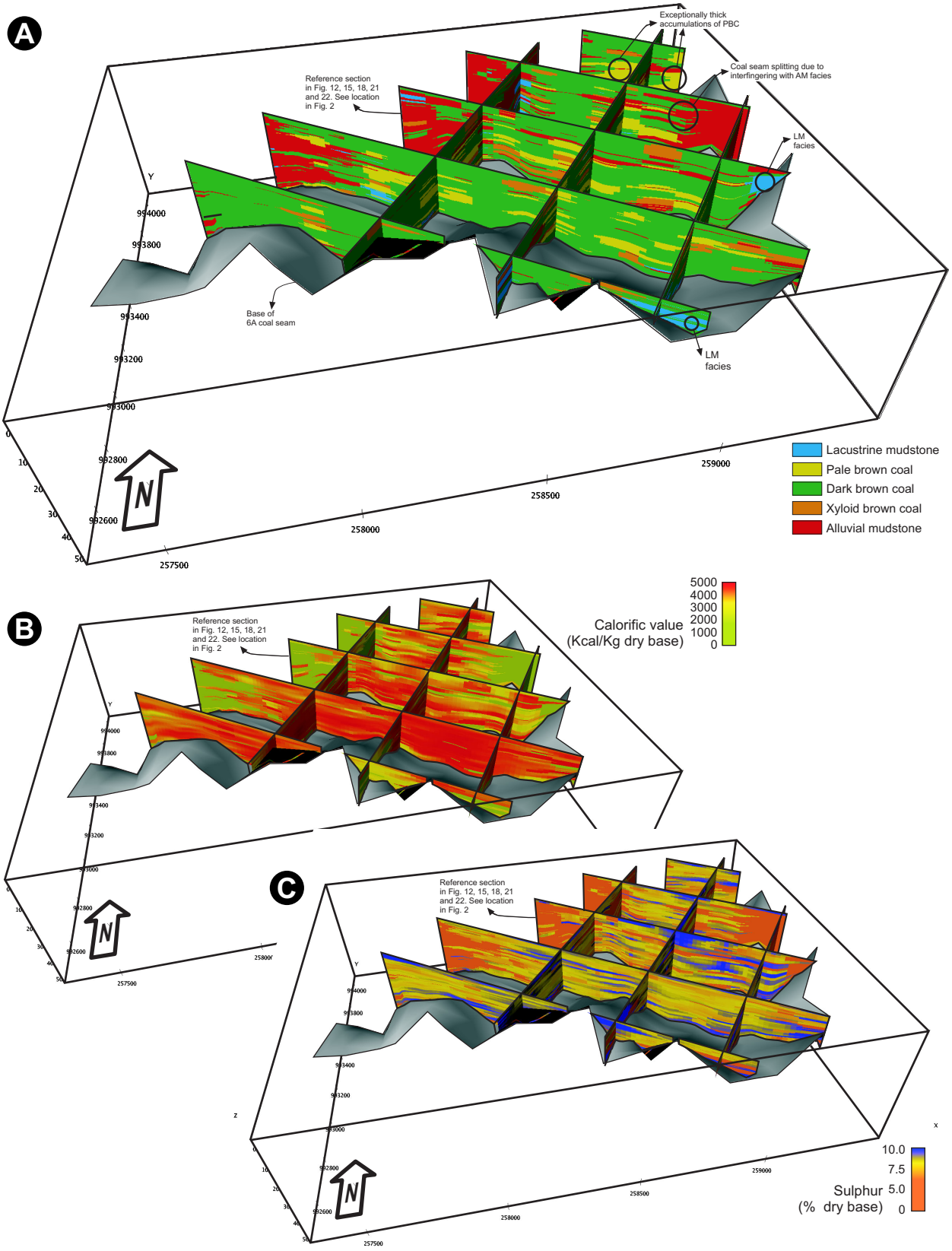

Figure 20. Fence diagrams viewed from the S showing 3D reconstructions of the 6AW zone. **(A)** Facies reconstruction using IK-T (NN set to 48 and a geological grid layering style). **(B)** Interpolation of calorific values using the facies distribution as a template. **(C)** Interpolation of total sulphur percentages using the facies distribution as a template. Vertical exaggeration 10x. See Figure 21 and 22, and supplementary material for further detail

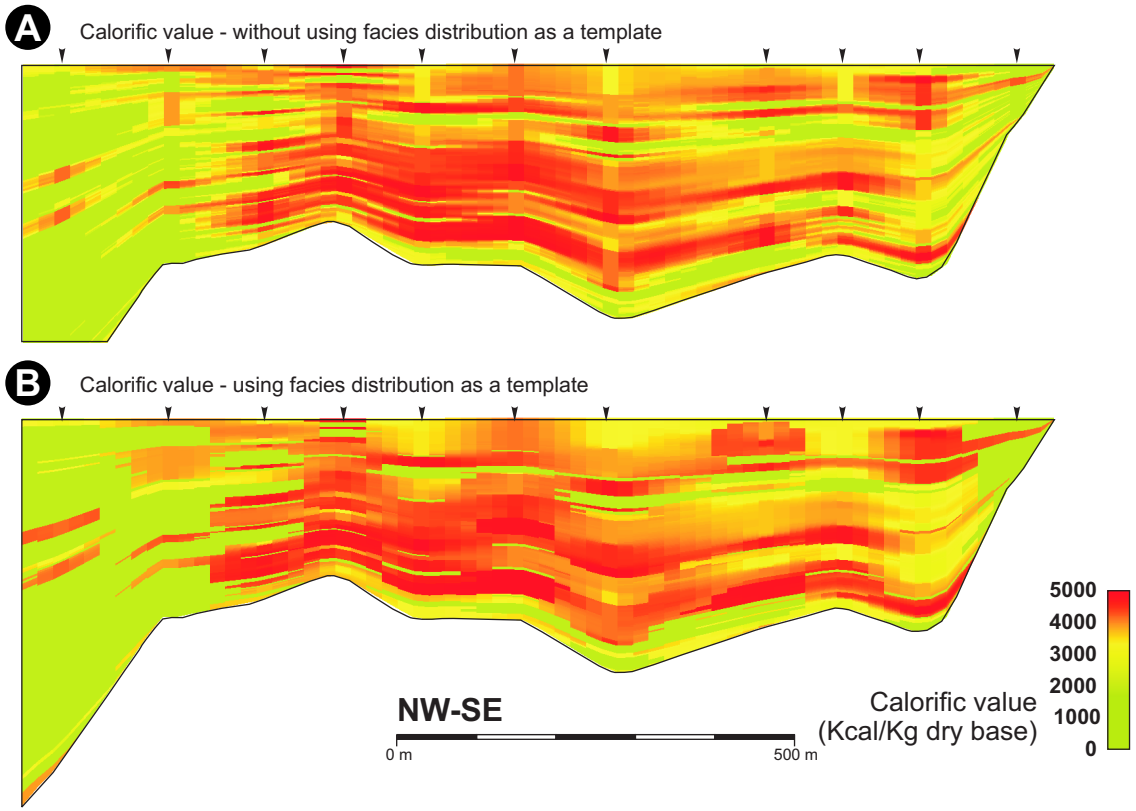

Figure 21: Reference section showing calorific value interpolations without using facies distribution as a template **(A)** and using facies distribution as a template **(B)**. See location of the section in Figure 2. Arrows indicate the position of intersected wells. Vertical exaggeration 10x.

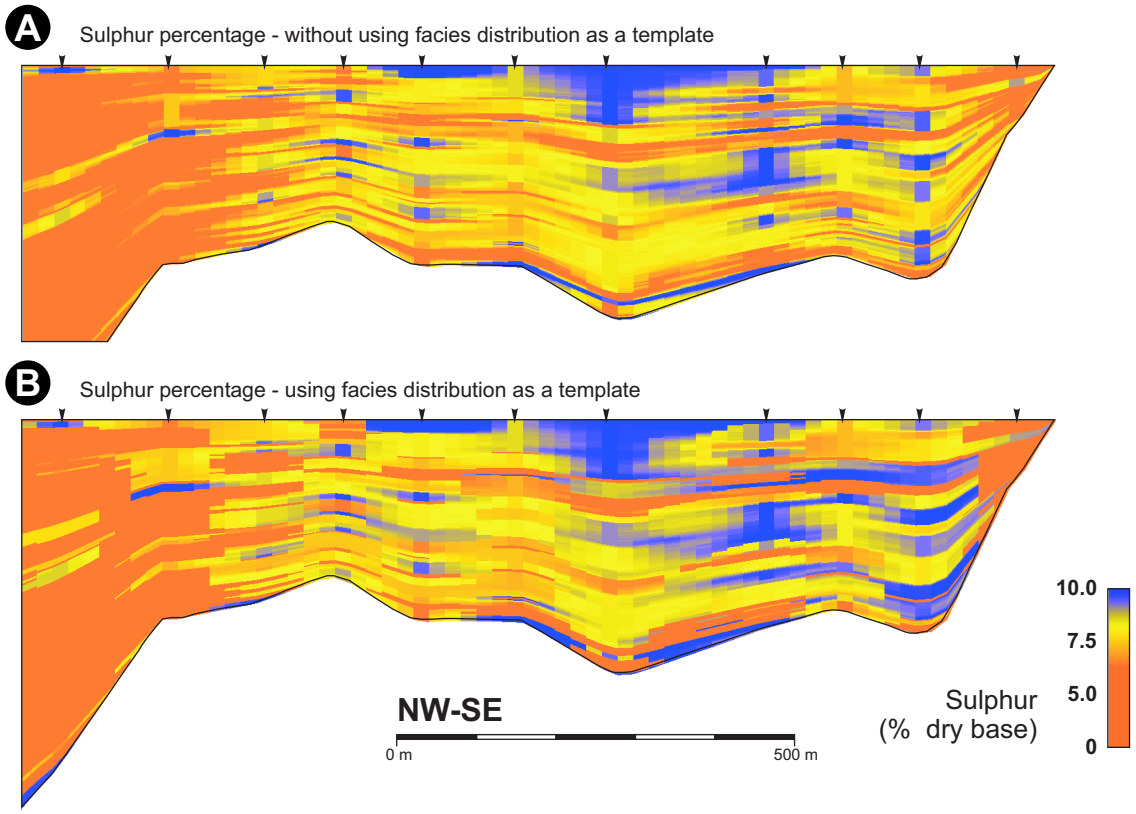

Figure 22: Reference section showing total sulphur percentage interpolations without using facies distribution as a template **(A)** and using facies distribution as a template **(B)**. See location of the section in Figure 2. Arrows indicate the position of intersected wells. Vertical exaggeration 10x.

		Approach to deal with the categorical property	
Weighting criteria	**Inclusion of areal trends**	Truncated Approach Methods	Indicator Approach Methods
Inverse of distance	Implicitly	Truncated Inverse Squared Distance Weighting (TISDW)	Indicator Inverse Squared Distance Weighting (IISDW)
Minimization of estimation variance	Implicitly	Truncated Kriging (TK)	Indicator Kriging (IK)
	Explicitly	Truncated Kriging with an areal Trend (TK-T)	Indicator Kriging with an areal Trend (IK-T)

Table 1: Classification of the interpolation methods compared. This classification is based on the approach to deal with the categorical property, the weighting criteria and the inclusion of trends.

A) Calorific value cross validation results

		Mean	Std. Dev.	Mean absolute error	Relative mean absolute error
True values		2968	1925		
CV estimates without using facies as a template		3316	1519	1181	40%
CV estimates using facies as a template	**Facies also cross-validated**	3117	1804	1060	36%
	Facies already known	3003	1897	324	11%

B) Sulphur percentage cross validation results

		Mean	Std. Dev.	Mean absolute error	Relative mean absolute error
True values		5.66	3.98		
CV estimates without using facies as a template		6.01	2.76	2.76	49 %
CV estimates using facies as a template	**Facies also cross-validated**	5.88	3.48	2.50	44 %
	Facies already known	5.52	3.56	1.06	19 %

Table 2: Cross validation results for calorific value (dry basis) **(a)** and total sulphur percentage (dry basis) **(b)**. See text for related discussion

the positions of the wells (Fig. 2). The horizontal grid spacing was set to 20 m. Each grid cell can only have one facies assigned to it; therefore, facies described in the cores were upscaled to the size of grid cells. This was conducted for each layering style and by assigning the most abundant logged facies to each cell. Upscaled categories were the input data for all subsequent interpolations.

3.4. Interpolation methods

The interpolation methods compared were based on: a) resolving the categorical property distribution as multiple truncations of a continuous property (truncated approach methods: truncated inverse squared distance weighting (TISDW), truncated kriging (TK), and truncated kriging with an areal trend (TK-T)), or b) on the indicator approach for categorical properties (indicator approach methods: indicator inverse squared distance weighting (IISDW), indicator kriging (IK), and indicator kriging with an areal trend (IK-T)) (Table 1). GSLIB code (Deutsch and Journel, 1998) was used for kriging-based methods; GSTAT package (Pebesma and Wesseling, 1998) was used for inverse distance-based methods.

3.4.1. Truncated approach methods

Methods based on the truncated approach start by transforming facies categories to a single continuous property. This requires a previous ordering of facies. In our case this was done following energy-related paleonvironment criteria (LM, PBC, DBC, XBC and AM). These methods compute the thresholds between facies; assuming a Gaussian distribution, the areas between thresholds correspond to the proportions measured in the upscaled well data (de Marsily, 1998). The next step is to assign to each facies a value

between their thresholds; constant values located in the centre of each category were used.

The continuous values assigned to well data were used to derive experimental variograms with standardized sills. Theoretical variogram models were adjusted to the experimental ones (Fig. 5). Differences in horizontal variograms along different azimuths were not significant, and thus, horizontal isotropic ranges were used. The vertical variogram sills did not reach the standard deviation of the continuous property (Fig. 5). This fact is explained by the presence of an areal trend, as not all the vertical wells encounter the full variability of facies distribution (Kupfersberger and Deutsch, 1999; Gringarten and Deutsch, 2001).

Interpolation of the continuous property was conducted using three different algorithms (inverse distance weighting, kriging, and kriging with an areal trend; see below). In all cases, the final step of truncated approach methods was to truncate the continuous property interpolation with the thresholds between facies categories.

Truncated inverse squared distance weighting (TISDW)

Interpolation of the continuous property was carried out using inverse squared distance weighting (Kane et al., 1982; Pebesma and Wesseling, 1998) and conditioned by the well data. As indicated by the relationship between vertical and horizontal variogram ranges (Fig. 5) an important geometric anisotropy exists (Kupfersberger and Deutsch, 1999). This anisotropy is typical of sedimentary deposits, and in inverse squared distance weighting was considered by multiplying the vertical coordinates by an anisotropy factor prior to the interpolation (Jones et al, 1986; Zoraster, 1996). In order to get a reasonable value for the anisotropy factor, the ratio between horizontal and vertical variogram ranges was used.

Truncated kriging (TK)

Interpolation of the continuous property was also carried out using ordinary kriging (Matheron, 1963; Journel and Huijberts, 1978; Cressie, 1990) and conditioned by the well data and the adjusted theoretical variograms (Fig. 5).

Truncated kriging with an areal trend (TK-T)

The presence of an areal trend (Gringarten and Deutsch, 2001), as demonstrated by vertical variograms not reaching the standard deviation of the continuous property (Fig. 5), motivated the use of an interpolation method considering this trend explicitly (TK-T). The areal trend was modelled following the decomposition into a mean and a residual, as suggested by Langlais et al (1993) and Deutsch (2002). The mean corresponds to a 2D map derived from the interpolation of averaged values of the continuous property along each well (Fig. 6). In the well data locations, the residual was obtained by subtracting the mean from the original transformed property.

Experimental variograms were derived from the residual property and standardized sills were used (Fig. 7). As expected, experimental vertical variograms of the residual property did not show strong indication of areal trends. Theoretical variogram models were adjusted to the experimental ones. Differences in horizontal variograms along different azimuths were not significant, and thus, horizontal isotropic ranges were used. Interpolation of the residual property was carried out using ordinary kriging (Matheron, 1963; Journel and Huijbregts, 1978; Cressie, 1990) and conditioned by the residual at well data locations and the adjusted theoretical variograms. The results of the residual property interpolations were added to the mean.

3.4.2. Indicator approach methods

When dealing with categorical properties like facies, the indicator approach (Journel, 1983; Gómez-Hernández and Srivastava, 1990) transforms each facies into a new property, and the value of each new property corresponds to the probability of finding the related facies at a given position. Where well data exist, the value of the property corresponding to the facies present was set to one, whereas the values of the other properties were set to zero.

The transformed well data were used to estimate indicator variograms for each facies. In the case of indicator variograms, non-standardized sills were used, as the sill of an indicator variogram is related to the percentage of each facies. The theoretical variogram models were adjusted to the experimental ones (Fig. 8). Depending upon the spatial continuity shown by each facies, the horizontal and vertical variogram ranges varied. For each facies, differences in horizontal variograms along different azimuths were not significant, and therefore, horizontal isotropic ranges were used. The vertical variograms sills did not reach the standard deviation of the indicator properties (Kupfersberger and Deutsch, 1999; Gringarten and Deutsch, 2001); this effect was larger for facies DBC and AM (Fig. 8C and 8E). As in the case of the continuous approach, vertical variograms not reaching the sill are related to the presence of an areal trend.

Again, interpolation of the indicator properties was conducted using three different algorithms (inverse distance weighting, kriging, and kriging with an areal trend; see below). Results from the interpolation of indicator properties corresponded to the probability of finding each facies at each grid cell, and the final step of indicator

approach methods was to select the facies with the highest probability of occurrence at each grid cell.

Indicator inverse squared distance weighting (IISDW)

Interpolation of each new indicator property was carried out using inverse squared distance weighting and conditioned by the transformed well data. As horizontal and vertical variogram ranges varied depending upon the facies (Fig. 8), geometric anisotropy and the ratio between horizontal and vertical range also varied. Therefore, different anisotropy ratios were used for each facies.

Indicator kriging (IK)

Interpolation of each new indicator property was also carried out using ordinary kriging (Matheron, 1963; Journel and Huijbregts, 1978; Cressie, 1990) and conditioned by the transformed well data and the theoretical indicator variograms (Fig. 8).

Indicator kriging with an areal trend (IK-T)

The presence of an areal trend (Gringarten and Deutsch, 2001), as demonstrated by vertical indicator variograms not reaching the sill value (Fig. 8), motivated the use of an interpolation method explicitly considering this trend (IK-T). Areal trends for each facies were modelled following the same approach as for the continuous approach.

For each new indicator property, 2D mean maps were derived from the interpolation of averaged values along each well (Fig. 9). These maps corresponded to the areal proportion of each facies, and showed a clear non-stationary distribution. In the well data locations, for each indicator property, residuals were obtained by subtracting the mean maps to the original indicator properties.

Experimental variograms were derived from the residual properties, each corresponding to a different facies, and standardized sills were used. As expected, experimental vertical variograms of the residual properties did not show strong indication of areal trends (Fig. 10). The theoretical variogram models were adjusted to the experimental ones (Fig. 10). Differences in horizontal variograms along different azimuths were not significant for each facies, and thus, horizontal isotropic ranges were used. Interpolation of the residual properties was carried out using ordinary kriging (Matheron, 1963; Journel and Huijberts, 1978; Cressie, 1990) and conditioned by the residual properties at well data locations and the adjusted theoretical variograms (Fig. 10). The results of the residual properties interpolations were added to the mean maps for each facies.

3.5. Searching conditions

Searching conditions refer to the number of neighbouring data points averaged to obtain each grid cell estimate (NN). In this study, octant restrictions were not used since the input well data was already distributed over a nearly regular grid. The seven different NN scenarios used were: 4, 12, 24, 48, 96, 192 and 288.

4. Methodology for comparison criteria

Interpolation strategies were compared based on the geological realism of facies reconstructions and CV results (i.e. looking for minimum CV error and minimum CV smoothing).

4.1. Definition of the cross validation error

Several variations in the CV procedure and the error definition exist (Davis, 1987; Isaaks and Srivastava, 1989). In the case of categorical properties defined from well data, the following procedure was used to cross validate the results. First, an entire upscaled well was temporally extracted from input data. Second, facies interpolations were carried out on the grid cells intersected by the extracted well using the remnant data. Third, the predicted facies distribution in the extracted well was compared to the true distribution. This procedure was repeated for all the wells. The probability of obtaining an erroneous facies prediction was obtained by averaging results for all the grid cells intersected by the wells. Each grid cell was assigned the same weight, independently of its thickness. This CV error definition is a variant of the commonly used mean absolute error (Zimmermann et al., 1999; Teegavarapu and Chandramouli, 2005) adapted to categorical variables defined in 3D by well data. In all cases, the theoretical variogram models fitted with the complete data set were used (Figs. 5, 7, 8 and 10). For interpolation methods using areal trends (TK-T and IK-T), the areal trends were derived from the remnant wells when computing CV results.

4.2. Cross validation error and smoothing effect

Smoothing effect related to each interpolation strategy (defined by grid layering style, interpolation method and searching conditions) influences the probability of an erroneous facies prediction. Smoothing was measured herein by measuring the proportion of the most extended category (DBC) predicted by CV. Proportion of DBC as estimated from CV was larger and directly related to the proportion of DBC as estimated from a complete 3D facies interpolation (Fig. 11A). This is because mean distances between cross-validated locations and averaged data points are always larger

in CV than mean distances between estimated grid cells and averaged data points for a facies interpolation along the entire grid. This increase in average distance limits the use of CV error as an exact measure for interpolation accuracy, even though it can be used as an approximation or as a relative measure for ranking interpolation strategies.

Considering randomly generated facies estimates, it can be observed that the probability of obtaining erroneous predictions decreases as the smoothing effect increases (Fig. 11B). However, excessive smoothing should be avoided, since it would imply an artificial increase in spatial continuity of the facies distributions and an additional decrease of global accuracy (Goovaerts, 1997; Journel et al., 2000; Yamamoto, 2005). For any given degree of smoothing, CV interpolation errors were in all cases lower than the errors obtained using randomly generated unconditioned facies estimates (Fig. 11B).

5. Results

Visual analysis and CV test was conducted for 168 different interpolation strategies (4 grid layering styles, 6 interpolation methods and 7 NN scenarios).

5.1. Grid layering style

Visual appearance of facies reconstructions considering different grid layering styles is markedly different (Fig. 12). Fig. 13A shows CV results for indicator approach methods considering different grid layering styles and intermediate NN (48).

At the same smoothing degree, each grid layering style yield different randomly estimated CV errors (Fig. 11B). This effect is due to the use of CV results not corrected for cell thickness. Actually, layering styles show small differences in the upscaled facies

proportions not corrected by cell thickness, these differences are perfectly correlated to CV error (Fig. 14). In order to compare CV errors from different grid layering styles, the bias introduced by computing CV results without weighting for true thickness was removed. This was achieved by dividing CV errors by the CV error obtained using estimates with total smoothing (DBC facies proportion at 100%, i.e. mean mapping) (Fig. 13B).

In terms of CV errors corrected for cell-thickness, the worst layering style is that parallel to the base, independently of the interpolation method and searching conditions (Fig. 13B). This fact quantitatively reflects the importance of considering a nearly horizontal layering style for interpolation; recall that interpolation is carried out considering the top of the interval as a horizontal datum.

Parallel to the top, proportional and geological grid layering styles yield similar errors, with rankings differing depending on the interpolation method considered. For IK and IIDW the smallest errors are obtained by the proportional layering (Fig. 13B), whereas for IK-T the smallest error is obtained for the layering parallel to the top (Fig. 13B).

Based upon geological knowledge of the coal zone deposition and post-depositional evolution of the basin (Cabrera et al., 1995; Ferrús, 1998; Santanach et al., 2005) it is reasonable to consider the presence of post-depositional folded stratification in the central parts and in the northern active basin margins (Fig. 1 and 2); that makes the proportional and geological grid layering styles more appropriate (Fig. 12C and D). Differences in the geological and proportional layering are mostly limited to the southern passive basin margin, being geological layering the most realistic, because it reproduces the onlap typical of expansive zones like 6AW (Fig. 12D).

5.2. Interpolation method and searching conditions

Fig. 15 shows facies reconstructions for the different interpolation methods. Fig. 16 and 17 show CV results for the different interpolation methods and using different NN. Interpolation methods can be ranked based on the results for the more realistic geological and proportional grid layering styles (section 5.1). In nearly all cases, rankings are also valid for the other two grid layering styles (parallel to the base and parallel to top). Results can be summarized as:

1) As expected (Herzfeld et al., 1993), CV smoothing increases as NN increases (Fig. 16).

2) Truncated approach methods yield CV estimates with higher smoothing (71-95%) than indicator approach methods (57-82%) (Fig. 16).

3) CV errors show different patterns depending upon the interpolation method approach (Fig 16). Truncated approach methods yield more restricted errors (from 43% to 49%), than indicator approach methods (from 39 to 52%).

4) Considering only truncated approach methods: a) for small NN (4-12), TISDW performs better than kriging-based methods (Fig. 17A); b) for intermediate NN (48), CV error for TISDW remains slightly smaller than kriging-based methods error, but the smoothing is greater (Fig. 17B); c) for large NN (192-288), kriging-based methods perform better than TISDW (Fig. 17C); and d) except for small NN, TK-T yield better results than TK (Fig 17).

5) Considering only indicator approach methods: a) for small NN (4-12), kriging-based methods yield the smallest CV error, whereas the lowest smoothing correspond to IISDW (Fig. 17A); b) for intermediate to large NN (48-288), kriging-

based methods have the lowest smoothing, whereas IISDW have the lowest CV error (Fig. 17B and 17C); and c) in all cases IK-T yields lower smoothing than IK, whereas CV error depend on the NN (Fig. 17), for low NN (4-12), CV error is smallest for IK-T; and for intermediate to high NN (48-288), CV error is smallest for IK.

6) Indicator approach methods perform better than truncated approach methods (Fig. 16). Visual comparison also supports this result (Fig. 15); the facies distributions obtained with indicator methods appear more heterogeneous and realistic.

5.3. Method robustness

To study the sensitivity of the resultant facies reconstructions to variations in the method input parameters, four different anisotropy scenarios were compared: 1) the first scenario corresponded to an overestimation of horizontal variogram ranges by a factor of two, 2) the second scenario to the actual values measured from input data, 3) the third scenario to an underestimation by a factor of two, and 4) the fourth scenario to an underestimation by a factor of ten. No uncertainty in vertical variogram ranges was considered since it is usually well constrained by vertical wells.

Fig. 18 and 19 show respectively facies reconstructions and CV results considering the different uncertainty scenarios. Only the results for indicator approach, kriging-based methods, assuming a geological and proportional layering, and using NN set to 48 are shown. Results for truncated approach methods and inverse distance-based methods are not presented due to their limited optimality (section 5.2). Intermediate NN (48) provides an optimum balance between visual results, CV error and smoothing effect (section 5.2 and 6.2).

Relatively small changes (scenario 1 and 3) to the anisotropy measured from well data (scenario 2) do not significantly alter the appearance of resultant facies distributions (Fig. 18A, B and C). The only differences correspond to restricted variations in the facies continuity, with the first scenario yielding the most continuous results. Variations in facies continuity have a moderate impact on CV smoothing and CV error (Fig. 19); changes in the anisotropy are inversely proportional to smoothing and directly proportional to CV error. The fourth scenario provides visually different results (Fig. 18D). This scenario yields the lowest CV error, but at expenses of a higher smoothing and a non-realistic appearance. In all the uncertainty scenarios, IK-T yields lower CV smoothing than IK, but at expenses of a slight increase in CV error (Fig. 19).

6. Discussion

6.1. Grid layering style

Layering was used to preset the surfaces along which facies should display larger continuity, and in this study demonstrated a critical influence on the resultant facies distributions appearance and realism (Fig. 12). Grid layering must be assumed and is only necessary when dealing with 3D geological properties. This assumption should be strongly supported by a previous geological knowledge of the bedding attitude. As has been shown, CV can be used to verify the idoneity of the definition of grid layering.

6.2 Interpolation method and searching conditions

Indicator approach methods rank as the optimum for facies interpolation of the 6AW coal zone. Truncated approach methods produce the worst results; these methods

are based on simplifying facies distribution to a single variable. This simplification imposes: 1) continuous facies ordering, and 2) use of only one variogram or anisotropy factor to characterize spatial variability, with all facies sharing the same anisotropy (de Marsily et al., 1998). Truncated approach methods are useful mainly in depositional settings with a highly ordered facies distribution. On the other hand, indicator approach methods allow more flexibility in defining the spatial variability of each facies separately, but at the cost of an increase in the number of input parameters and the computing time roughly proportional to the number of facies considered.

Results for different indicator approach methods are very similar. From the visual comparison (Fig. 15) it was difficult to choose an optimal method. Method ranking using CV results is very sensitive to changes in NN. IIDW is the most sensitive method to variations in NN (Fig. 16). Similar results have been reported for interpolation dealing with continuous variables (Weber and Englund, 1992 and 1994). IK and IK-T are also sensitive to NN, but their CV error and CV smoothing stabilise beyond and intermediate NN (NN = 48, Fig. 16). Therefore indicator approach kriging-based methods were the preferred for facies interpolation (Fig. 17).

One of the most important advantages of kriging-based methods with respect to simpler inverse distance-based methods is the ability to take into account the relative positions of sampling data in order to select an optimal weighting scheme. This advantage is more significant when intermediate to high NN are considered. In addition, if input data were more irregularly distributed, differences in performance between kriging-based methods and inverse distance-based methods would increase.

An intermediate number of nodes (48) was chosen as an optimum compromise to minimize both CV error and smoothing effect (Fig. 16), and at the same time

obtaining a realistic facies distribution (Fig. 15). Using larger NN also implies a dramatically increase in computing time.

IK-T does not yield significantly better CV results than IK despite the presence of marked non-stationary facies distributions (i.e. areal trends). This agrees with results by Journel and Rossi (1989) dealing with a continuous variable. These authors stated that when interpolating using a limited NN, explicitly considering a trend does not significantly improve results obtained without explicitly considering the trend. This happens because in the latter case the trend is implicit when using a limited NN. Explicitly considering a trend proves more useful for extrapolation. In our study, the use of a trend with intermediate to large NN values (NN over 48) results in a diminution of CV smoothing, but at the expenses of a slight increase in CV error. The diminution of smoothing effect produced by the IK-T makes us consider it the optimum method for facies interpolation. The slight increase in CV error when explicitly using the trend agrees with the results by Zimmermann et al. (1999) dealing with a complex continuous variable.

6.3. Method robustness

Moderate errors in the determination of anisotropy (up to an overestimation or underestimation by a factor of two) do not significantly alter the results, confirming the robustness of the interpolation method. Large errors in the determination of anisotropy, particularly when corresponding to an underestimation, cause a large impact on the geological realism of the resultant facies distribution. However, such large errors are not likely to occur because interpolation is considered useful only when dense well data coverage is available, permitting a reasonable approximation to anisotropy. Hard data is the most important input for conditioning interpolation results.

6.4 The resulting 3D facies reconstruction

Once an optimum and robust 3D facies interpolation strategy was determined (IK-T using NN set to 48 and a geological grid layering style), the resultant 3D facies reconstruction was analysed. This reconstruction (Fig. 20A) allows a better understanding of spatial and geometrical relationships of facies (vertical and lateral changes, lateral continuity, coal seam splitting, etc).

The interaction between alluvial fans and the mire and lacustrine zones was the main factor controlling the areal development of the 6AW coal seam and the seam splitting by siliciclastic inputs. The areal distribution of the main environments in the coal zone (distal alluvial fan, marsh, swamp and lacustrine) varied during its deposition. These variations depended on the balance between allogenic factors (climate, tectonics and the resulting water and detritic inputs), as well as on the autogenic alluvial fan and mire evolution (Cabrera et al., 1995; Ferrús, 1998).

AM facies deposited in the distal and marginal zones of the alluvial fans that spread into the basin from its margins. Consequently this facies fringes the seam boundaries, particularly in the northern and eastern active basin margins, where small, fine-grained dominated alluvial fans developed related to tectonic structures (Fig. 1D and Fig. 20A). AM facies interfinger and even spread into the inner coal seam zone, causing its splitting. The 3D facies reconstruction allows us to recognize and trace these splitting zones precisely. This analysis is a powerful previous step to the accurate prediction and evaluation of the coal/mudstone rate changes that often occur as mining advances (Fig. 20A).

LM facies occur as isolated pods scattered along some marginal basin zones (Fig. 20A). The development and persistence of the small lakes where LM facies

deposited was probably favoured by a larger subsidence/sedimentation rate produced along the northern and eastern tectonic basin margins. However, their occurrence along the non-tectonically active southern margin also suggests the influence of other factors not yet fully understood. The resulting 3D reconstruction shows the occurrence of these coal barren zones that must be preventively considered during mining operations.

DBC facies makes up most of the coal seam and constitutes the dominant background. DBC beds are thick and laterally extensive and may spread all over the extent of the seam zone (Fig. 20A). PBC facies are a less important component in the seam zone. This facies often makes up laterally extensive but lenticular bodies that are embedded in the DBC dominated sequences. Exceptionally thick and persistent, laterally more restricted PBC sequences appear in the northeastern basin margin (Fig. 9 and 20A), which corresponds to one of the most subsiding areas during deposition of 6AW. The shallow subaqueous conditions suitable for deposition of PBC facies would developed persistently in this notheastern margin (where PBC attains its maximum thickness), and in some of the inner parts of the seam, far away from the detritic inputs that filled up the aquatic zones and prevented aquatic peat accumulation. The limited horizontal continuity of PBC facies is revealed by the 3D reconstruction and agrees well with the relatively small horizontal indicator variogram range (Fig. 8B). The XBC facies appears even as more randomly distributed than DBC and PBC and make up laterally restricted and mostly thin bodies (Fig. 20A). This conspicuous random distribution pattern accords well with the environmental conditions and processes that resulted in its deposition.

It is not possible to establish an obvious basinwide sequence evolutionary trend considering the relative DBC, PBC and XBC facies succession and development. In fact the local sequence evolutionary patterns are quite diverse in the different basin zones.

From this point of view the obtained 3D reconstruction arises as a powerful tool to capture the diverse facies distribution and the local variations of the facies-related coal properties (see section 6.5).

6.5. Interpolation of coal quality properties based on the 3D facies reconstruction

The facies reconstruction was also applied as a template to improve the realism and accuracy of coal quality property interpolations; this makes sense only when these properties depend at some extent on the facies category. In the case of the 6AW coals, a relationship between facies and calorific value (on a dry base) (Fig. 3A), and facies and total sulphur percentage (on a dry base) was observed (Fig. 3B).

Calorific value and total sulphur percentage interpolations were carried out using kriging with NN set to 48 and assuming a geological grid layering style. Two different interpolation strategies were compared: 1) interpolating the measured values of coal properties directly, without using facies as a template; and 2) interpolating facies and using the interpolated facies as a template to interpolate the values of the coal properties (i.e. taking into account the interpolated facies distribution in order to restrict averaged data points to those neighbours belonging to the same facies, Fig. 20B and C). Cross sections of the 3D interpolations are presented in Fig. 21 and 22. CV was used to quantitatively discriminate which strategy provides the most accurate coal property interpolations. When considering facies as a template two options were compared: a) using also cross-validated facies, and b) considering facies in the cross-validated well as already known.

The interpolations using facies as a template provide better CV results than the interpolations obtain without using facies (Table 2). Results using facies as a template

yield the lowest differences between the true mean and the interpolated distribution mean (conditional bias) and the true standard deviation and interpolated standard deviation (smoothing). Results using facies as a template also yield the lowest mean absolute error and relative mean absolute error (accuracy). CV results considering already known facies in the cross-validated wells are even better than the CV results using also cross-validated facies. The lower relative mean absolute errors yielded by calorific value respect to sulphur percentage (Table 2) is related to the fact that calorific value is better correlated to facies than sulphur, which is highly influenced by other factors (i.e. amount of sulphate inputs and redox conditions in each subbasin zone).

7. Conclusions

1) 3D interpolation permits the correlation of facies in a large number of wells. This technique proves to be useful when facies distribution is reasonably well captured by dense well data coverage.

2) Visual appearance and cross validation (CV) results prove to be valid tools to compare and rank different categorical property interpolation strategies and input parameter uncertainty scenarios. CV error is affected by the interpolation smoothing and tends to decrease as the smoothing increases.

3) The optimal and most robust facies interpolation strategy for the chosen case study (6AW coal seam zone, As Pontes basin) is indicator kriging with an areal trend (IK-T), using a number of data points averaged to obtain each estimate (NN) set to 48, and using a geological grid layering style.

4) An accurate definition of the grid layering style, based on *a priori* geological knowledge, prove very important to generate realistic facies reconstructions.

5) The indicator approach methods provide visually similar facies distributions. Results of indicator kriging (IK) are slightly less robust to variations in the input method parameters than results of IK-T, and indicator inverse squared distance results are more sensitive to variations in searching conditions than IK and IK-T. Truncated approach methods yield the worst results.

5) Smoothing effect increases with NN; intermediate NN values provide an optimum compromise between CV error, CV smoothing and computing time.

7) 3D interpolations provide a useful representation of facies distribution, which enables a better understanding of spatial and geometrical aspects of facies distribution in the coal seam zone.

8) As sulphur percentage and calorific value depend at some extent on coal facies, 3D facies reconstructions enables a more accurate interpolation of these properties.

9) This work demonstrates how 3D facies reconstructions are suitable and advisable for optimising coal exploration and mining in extensively drilled and sampled, thick and heterogeneous coal seam zones. Such reconstructions would help in planning selective mining according to the facies distribution and their related properties.

8. Acknowledgements

This research was carried out in the Geomodels Institute. This institute is sponsored by Generalitat de Catalunya (DURSI) and Instituto Geologico y Minero de España (IGME) and includes the 3D Geological Modelling CER (University of Barcelona). The authors are indebted to ENDESA MINA PUENTES for providing the dataset; its department of geology is also acknowledged for friendly support and field guidance. Financial support from the MEyC (Proyectos CARES BTE 2001-3650 and MARES CGL 2004-05816-C02-02/BTE) and from the Generalitat de Catalunya (Grup de Recerca de Geodinàmica i Anàlisi de Conques, 2005SGR-000397) is acknowledged. O. Fernández and Y. Almar are acknowledged for the review of a preliminary manuscript. Research by O. Falivene is funded by a pre-doctoral grant from the Spanish Government (Ministerio de Educación y Ciencia). Roxar is thanked for providing the IRAP RMS reservoir modelling software.

9. References

Bacelar, J., Alonso, M., Kaiser, C., Sánchez, M., Cabrera, L., Sáez, A., Santanach, P., 1988. La Cuenca Terciaria de As Pontes (Galicia): su desarrollo asociado a inflexiones contractivas de una falla direccional, Simposio sobre Cuencas en régimen transcurrente. Sociedad Geologica de España, pp. 113-121.

Bancroft, B.A., Hobbs, G.R., 1986. Distribution of kriging error and stationarity of the variogram in a coal property. Mathematical Geology 18, 635-652.

Boman , G., Molz, F.J., Guven, O., 1995. An evaluation of interpolation methodologies for generating three-dimensional hydraulic property distributions from measured data. Ground Water 33, 247-258.

Borga, M., Vizzaccaro, A., 1997. On the interpolation of hydrologic variables: formal equivalence of multiquadratic surface fitting and kriging. Journal of Hydrology 195, 160-171.

Brummert, A.C., Pool, S.E., Portman, M.E., Hancock, J.S., Ammer, J.R., 1991. Determining optimum estimation methods for interpolation and extrapolation of reservoir properties: a case study, in: Lake, L.W., Carroll, H.B., Wesson (Eds.), Reservoir Characterization, pp. 445-485.

Cabrera, L., Ferrús, B., Sáez, A., Santanach, P., Bacelar., J., 1996. Onshore Cenozoic strike-slip basins in NW Spain, in: Friend, P.F., Dabrio, C.J. (Eds.), Tertiary Basins of Spain, the Stratigraphic Record of Crustal Kinematics, pp. 247-254.

Cabrera, L., Hagemann, H.W., Pickel, W., Sáez, A., 1992. Caracterización Petrológica y Geoquímica Orgánica de los lignitos de la cuenca de As Pontes (La Coruña), II Congreso Geológico de España - VIII Congrso Latinoamericano de Geología. Tomo 2. Simposio sobre Geología del carbón, pp. 239-246.

Cabrera, L., Hagemann, H.W., Pickel, W., Sáez, A., 1995. The coal-bearing, Cenozoic As Pontes Basin (northwestern Spain): geological influence on coal characteristics. International Journal of Coal Geology 27, 201-226.

Cavagnetto, C., 2002. La plynoflore du Bassin d'As Pontes en Galice dans le Nord Ouest de l'Espagne à la limite Rupélien-Chattien (Oligocène). Palaeontographica. Abteilung B: Paläophytologie 263, 161-204.

Cressie, N., 1990. The origins of kriging. Mathematical Geology 22, 239-252.

Davis, B.M., 1987. Uses and abuses of cross-validation in geostatistics. Mathematical Geology 19, 241-248.

Davis, B.M., Greenes, K.A., 1983. Estimation using spatially distributed multivariate data: An example with coal quality. Mathematical Geology 15, 287-300.

de Marsily, G., Delay, F., Gonçalves, J., Renard, P., Teles, V., Violette, S., 2005. Dealing with spatial heterogeneity. Hydrogeology Journal 13, 161-183, DOI 110.1007/s10040-10004-10432-10043.

de Marsily, G., Delay, F., Teles, V., Schafmeister, M.T., 1998. Some current methods to represent the heterogeneity of natural media in hydrogeology. Hydrogeology Journal 6, 115-130.

Deutsch, C.V., 2002. Geostatistical Reservoir Modeling. Oxford, 376 pp.

Deutsch, C.V., Journel, A.G., 1998. GSLIB: Geostatistical Software Linrary and User's Guide, 2nd edition. Oxford University Press, 350 pp.

Dirks, K.N., Hay, J.E., Stow, C.D., Harris, D., 1998. High-resolution studies of rainfall on Norfolk Island Part II: interpolation of rainfall data. Journal of Hydrology. 208, 187-193.

Ferrús, B., 1998. Análisis de cuenca y relaciones tectónica-sedimentación en la cuenca de As Pontes (Galícia). University of Barcelona (Spain).

Gómez-Hernández, J., Srivastava, R.M., 1990. ISIM 3D: an ANSI-C three-dimensional and multiple indicator conditional simulation program. Computers & Geosciences 16, 355-410.

Goovaerts, P., 1997. Geostatistics for natural resources evaluation, New York, 483 pp.

Goovaerts, P., 2000. Geostatistical approaches for incorporating elevation into the spatial interpolation of rainfall. Journal of Hydrology 228, 113-129.

Gringarten, E., Deutsch, C.V., 2001. Variogram interpretation and modeling. Mathematical Geology 33, 507-535.

Hagemann, H.W., Pickel, W., Cabrera, L., Sáez, A., 1997. Tertiary lignites of the As Pontes (NW Spain) - An example for composition of bright coal layers and its implications for formation, Proceedings of the 9th International Conference on Coal Science, 1: 31-34.

Herzfeld, U.C., Eriksson, M.G., Holmund, P., 1993. On the Influence of Kriging Parameters on the Cartographic Output - A Study in Mapping Subglacial Topography. Mathematical Geology 25, 881-900.

Hohn, M.E., McDowell, R.R., 2001. Uncertainty in Coal Property Valuation in West Virginia: a case study. Mathematical Geology 33, 191-217.

Huerta, A., 1998. PhD Tesis. Petrografía, Mineralogía y Geoquímica de los lignitos de la cuenca Oligo-Miocena de As Pontes (A Coruña): Control geológico sobre la calidad del carbon, Universitat de Barcelona, pp. 333.

Huerta, A., 2001. Resumen de tesis Doctoral: Caracterización mineralógica y geoquímica de los lignitos de la cuenca Terciaria de As Pontes (Provincia de La Coruña). Acta Geológica Hispánica 36.

Huerta, A., Querol, X., Sáez, A., Cabrera, L., 1997. Mineralogy and Geochemistry of the As Pontes lignites (NW Spain): Relation with paleohydrological basin evolution. Migration and Interaction in Sedimentary basins and Orogenic Belts. GEOFLUIDS II'97. Contributions to the Second International Conference on Fluid Evolution. Geological Society Special Publication, pp. 370-373.

Isaaks, E.J., Srivastava, R.M., 1989. An introduction to Applied Geostatistics. Oxford University Press, 561 pp.

Jones, T.A., 1988. Geostatistical Models with Stratigraphic Control - Short Note. Computers & Geosciences 14, 135-138.

Jones, T.J., Hamilton, D.E., Johnson, C.R., 1986. Contouring geologic surfaces with the computer. Van Nostrand Reinhold, New York.

Journel, A., 1986. Geostatistics: Models and Tools for the Earth Sciences. Mathematical Geology 18, 119-140.

Journel, A., Kyriakidis, P.C., Mao, S., 2000. Correcting the Smoothing Effect of Estimators: A Spectral Postprocessor. Mathematical Geology 32, 787-813.

Journel, A.G., 1983. Nonparametric Estimation of Spatial Distributions. Mathematical Geology 15, 445-468.

Journel, A.G., Huijbregts, C.J., 1978. Mining geostatistics. Academic Press, 600 pp.

Journel, A.G., Rossi, M., 1989. When do we need a trend in kriging? Mathematical Geology 21, 715-739.

Kane, V.E., Begovich, C.L., Butz, T.R., Myers, D.E., 1982. Interpretation of Regional Geochemistry Using Optimal Interpolation Parameters. Computers & Geosciences 8, 117-135.

Kupfersberger, H., Deutsch, C.V., 1999. Methodology for Integrating Analog Geologic Data in 3-D Variogram Modeling. American Association of Petroleum Geologists Bulletin 83, 1262-1278.

Langlais, V., Doyle, J.D., Sweet, M.L., Geehan, G., 1993. An additional geological input to SIS: the vertical organization of lithofacies, in: Eschard, R., Doliguez, B. (Eds.), Subsurface Reservoir Characterization from Outcrop Observations. Editions Technip, Paris, pp. 111-123.

Matheron, G., 1963. Principles of geostatistics. Economic Geology 58, 1246-1266.

Moyeed, R.A., Papritz, A., 2002. An Empirical Comparision of Kriging Methods for Nonlinear Spatial Point Prediction. Mathematical Geology 34, 365-386.

Pebesma, E.J., Wesseling, C.G., 1998. GSTAT: A program for geostatistical modelling, prediction and simulation. Computers & Geosciences 24, 17-31.

Rouhani, S., 1986. Comparative study of ground-water mapping techniques. Ground Water 24, 207-216.

Sáez, A., Cabrera, L., 2002. Sedimentological and paleohydrological responses to tectonics and climate in a small, closed, lacustrine system: Oligocene As Pontes Basin (Spain). Sedimentology 49, 1073-1094.

Santanach, P., Baltuille, J.M., Cabrera, L., Monge, C., Sáez, A., Vidal-Romaní, J.R., 1988. Cuencas terciarias gallegas relacionadas con corredores de fallas direccionales, Simposio sobre: Aportación al Programa Internacional de Correlación Geológica. Sociedad Geologica de España, pp. 123-133.

Santanach, P., Ferrús, B., Cabrera, L., Sáez, A., 2005. Origin of a restraining bend in an evolving strike-slip system: The Cenozoic As Pontes basin (NW Spain). Geologica Acta 3, 225-239.

Schuenemeyer, J.H., Power, H., 2000. Uncertainty estimation for resource assessment - an application to coal. Mathematical Geology 32, 521-541.

Starks, T.H., Behrens, N.A., Fang, J.H., 1982. The combination of sampling and kriging in the regional estimation of coal resources. Mathematical Geology 14, 87-106.

Teegavarapu, R.S.V., Chandramouli, V., 2005. Improved weighting methods, deterministic and stochastic data-driven models for estimation of missing precipitation records. Journal of Hydrology 312, 191-206.

Tercan, A.E., Karayigit, A.I., 2001. Estimation of lignite reserve in the Kalburcayiri field, Kangal basin, Sivas, Turkey. International Journal of Coal Geology 47, 91-100.

Turner, B.R., Richardson, D., 2004. Geological controls on the sulphur content of coal seams in the Northumberland Coalfield, Northeast England. International Journal of Coal Geology 60, 169-196.

Watson, W.D., Ruppert, L.F., Bragg, L.J., Tewalt, S.J., 2001. A geostatistical approach to predicting sulfur content in the Pittsburgh coal bed. International Journal of Coal Geology 48, 1-22.

Weber, D.D., Englund, E.J., 1992. Evaluation and comparison of spatial interpolators. Mathematical Geology 24, 381-391.

Weber, D.D., Englund, E.J., 1994. Evaluation and comparision of spatial interpolators II. Mathematical Geology 26, 589-603.

Yamamoto, J.K., 2005. Correcting the Smoothing Effect og Ordinary Kriging Estimates. Mathematical Geology 37, 69-94.

Zimmerman, D., Pavlik, C., Ruggles, A., Armstrong, P., 1999. An experimental comparision of ordinary and universal kriging and inverse distance weighting. Mathematical Geology 31, 375-390.

Zoraster, S., 1996. Imposing Geologic Interpretarions on Computer-Generated Contours Using Distance Transformation. Mathematical Geology 28, 969-985.

Figure Captions

Figure 1. Geological setting and characteristics of the As Pontes basin. **(A)** Location of the As Pontes basin. **(B)** Geological map of the basin showing the main tectonic structures that affect the basement. Note the strike-slip fault and associated thrusts, which bound the northern basin margin; the N–S oriented normal faults and the E–W and NE–SW oriented thrusts. **(C)** Longitudinal sketch of the basin showing the main stratigraphic units, sedimentary facies and basement structures (see arrows for location on 1B), notice the stratigraphic position of the 6AW coal zone. **(D)** Paleogeographic sketches of the basin during deposition of the 6A interval.

Figure 2. Well location in the studied part of 6AW zone. Location of the NW-SE reference section that is used as an example in Figures 4, 12, 15, 18, 21 and 22 is shown. Coordinates in the lower left frame are in kilometres. See Figure 1B and 1D for structural details.

Figure 3. Relative frequency of calorific values **(A)** and sulfur percentages **(B)** in the three major coal facies in the 6AW coal seam zone. Plotted information corresponds to the core data upscaled to the size of grid cells. These were computed biased to the facies logs and assuming a geological layering (see section 5.1). Upscaled data (see section 3.3) are close to the original because of the fine grid used. Original data consisted in more than 2500 analyses (513 in PBC, 1840 in DBC, and 227 in XBC) for each property.

Figure 4. Reference section showing the different grid layering styles used for facies interpolations. See location of the section in Figure 2. Note that only one tenth of the grid layers is shown as reference. Vertical exaggeration 10x.

Figure 5. Standardized variograms for the transformed Gaussian property. Grey dots and dashed curves correspond to the experimental variograms derived from upscaled well data. No significant differences were observed in the experimental variograms derived from the four different grid layering styles. Continuous curves correspond to the theoretical model fitted (Hr and Vr stands for horizontal and vertical variogram ranges respectively):

$\gamma(h) = 0.6 \cdot \text{Exp}\ (Hr = 500m, Vr = 1.4m) + 0.4 \cdot \text{Exp}\ (Hr = 100m, Vr = 3m)$.

Figure 6. Areal trend derived from the interpolation of averaged values of the continuous property values along each well. The different shades reflect the average facies along each well. A clear non-stationary facies distribution is shown. Higher values are located predominantly near the basin margins (specially in the northern) where facies AM dominates. Intermediate-low values occur in the centre of the coal zone where facies DBC dominates. The lower values are restricted to some zones with dominance of facies PBC and LM.

Figure 7. Standardized variograms for the residual of the transformed continuous Gaussian property. Grey dots and dashed curves correspond to the experimental variograms derived from upscaled well data. No significant differences were observed in the experimental variograms derived from the four different layering styles.

Continuous curves correspond to the theoretical model fitted (Hr and Vr stands for horizontal and vertical variogram ranges respectively):
γ (h) = 0.6·Exp (Hr = 400m, Vr = 1.4m) + 0.4·Exp (Hr= 100m, Vr =3m).

Figure 8. Non-standardized indicator variograms assuming a geological layering. Grey dots and dashed curves correspond to the experimental variograms derived from upscaled well data. No significant differences were observed in the experimental variograms derived from the four different layering styles. Continuous curves correspond to the theoretical models fitted (Hr and Vr stands for horizontal and vertical variogram ranges respectively):
γ (h) LM = 0.018·Exp (Hr = 500m, Vr = 1.4m) + 0.012·Exp (Hr = 100m, Vr =3m).
γ (h) PBC = 0.063·Exp (Hr = 200m, Vr = 1.4m) + 0.042·Exp (Hr = 100m, Vr =3m).
γ (h) DBC = 0.150·Exp (Hr = 500m, Vr = 1.4m) + 0.100·Exp (Hr = 100m, Vr =3m).
γ (h) XBC = 0.039·Exp (Hr = 300m, Vr = 1.4m) + 0.026·Exp (Hr = 100m, Vr =3m).
γ (h) AM = 0.113·Exp (Hr = 700m, Vr = 1.4m) + 0.076·Exp (Hr = 100m, Vr =3m).

Figure 9. Areal trends for each indicator property derived from the interpolation of averaged values along each well. The maps correspond to the areal proportions of each facies. Note the difference in the range of the greyscale among the different facies.

Figure 10. Standardized variograms for the residual of the indicator properties, assuming a geological layering. Grey dots and dashed curves correspond to the experimental variogram derived from upscaled well data. No significant differences were observed in the experimental variograms derived from the four different layering styles. Continuous curves correspond to the theoretical models fitted (Hr and Vr stands for horizontal and vertical variogram ranges respectively):
γ (h) LM = 0.6·Exp (Hr = 500m, Vr = 1.4m) + 0.4·Exp (Hr = 100m, Vr =3m).
γ (h) PBC = 0.6·Exp (Hr = 200m, Vr = 1.4m) + 0.4·Exp (Hr = 100m, Vr =3m).
γ (h) DBC = 0.6·Exp (Hr = 500m, Vr = 1.4m) + 0.4·Exp (Hr = 100m, Vr =3m).
γ (h) XBC = 0.6·Exp (Hr = 300m, Vr = 1.4m) + 0.4·Exp (Hr = 100m, Vr =3m).
γ (h) AM = 0.6·Exp (Hr = 700m, Vr = 1.4m) + 0.4·Exp (Hr = 100m, Vr =3m).

Figure 11. (A) Relationship between DBC proportion predicted by CV and by the interpolation along the entire grid. Results shown correspond to a geological grid layering style and NN set to 48. **(B)** CV errors and smoothing using randomly generated unconditioned facies estimates, each line corresponds to a different grid layering style and was generated through the linear regression of the results for 100 realizations with varying DBC proportion, correlation factor (R2) was in all cases above 0.99.

Figure 12. Reference section showing facies distribution obtained by using different grid layering styles. In all frames the interpolation method used was indicator kriging with an areal trend (IK-T) and NN set to 48. See location of the section in Figure 2. Arrows indicate the position of intersected wells. Vertical exaggeration 10x.

Figure 13. (A) Relationship between DBC proportion predicted by CV (smoothing effect) and CV error for the different grid layering styles tested. Only results for indicator approach methods and NN set to 48 are shown; results for truncated approach methods are not presented due to their limited performance (section 5.2), intermediate NN (48) provided a good balance between visual results, CV error and smoothing (section 5.2). **(B)** Relationship between smoothing effect, and CV error divided by the

CV error obtained with total smoothing (DBC facies proportion at 100%, i.e. mean mapping).

Figure 14. Relationship between the original upscaled DBC proportion and the CV error using facies estimates with total smoothing (DBC facies proportion at 100%, i.e. Mean mapping) for the different grid layering styles.

Figure 15. Reference section showing facies distribution obtained by using different interpolation methods assuming a geological grid layering style. In all cases NN was set to 48. See location of the section in Figure 2. Arrows indicate the position of intersected wells. Vertical exaggeration 10x.

Figure 16. Relationship between DBC proportion predicted by CV (smoothing effect) and CV error for each interpolation method compared, considering geological (A) and proportional (B) grid layering styles. Results for different NN (4, 12, 24, 48, 96, 192 and 288) are shown.

Figure 17. Relationship between DBC proportion predicted by CV (smoothing effect) and CV error for each interpolation method compared, geological and proportional grid layering styles, and different NN set ups: 12 **(A)**, 48 **(B)** and 192 **(C)**.

Figure 18. Reference section showing facies distribution obtained by changing horizontal variogram ranges. In all frames the interpolation method used was indicator kriging with an areal trend (IK-T) and NN was set to 48. See location of the section in Figure 2. Arrows indicate the position of intersected wells. Vertical exaggeration 10x

Figure 19. Relationship between DBC proportion predicted by cross validation CV (smoothing effect) and CV error for each scenario of horizontal variogram range uncertainty.

Figure 20. Fence diagrams viewed from the S showing 3D reconstructions of the 6AW zone. **(A)** Facies reconstruction using IK-T (NN set to 48 and a geological grid layering style). **(B)** Interpolation of calorific values using the facies distribution as a template. **(C)** Interpolation of total sulphur percentages using the facies distribution as a template. Vertical exaggeration 10x. See Figure 21 and 22, and supplementary material for further detail.

Figure 21. Reference section showing calorific value interpolations without using facies distribution as a template **(A)** and using facies distribution as a template **(B)**. See location of the section in Figure 2. Arrows indicate the position of intersected wells. Vertical exaggeration 10x.

Figure 22. Reference section showing total sulphur percentage interpolations without using facies distribution as a template **(A)** and using facies distribution as a template **(B)**. See location of the section in Figure 2. Arrows indicate the position of intersected wells. Vertical exaggeration 10x.

Table Captions

Table 1: Classification of the interpolation methods compared. This classification is based on the approach to deal with the categorical property, the weighting criteria and the inclusion of trends.

Table 2: Cross validation results for calorific value (dry basis) **(a)** and total sulphur percentage (dry basis) **(b)**. See text for related discussion

Supplementary Material

Facies_IK-T_Geo_NN48.wrl file: virtual reality file with 3D view in Figure 20A

PCAdb_using facies.vrl file: virtual reality file with 3D view in Figure 20B

SULdb_using facies.wrl: virtual reality file with 3D view in Figure 20C

corvrml.exe file: executable file with the Cortona VRML Client (by Parallel Graphics©) for navigating .vrl files with Internet Explorer